International Journal of Engineering Science 217 (2025) 104378

Contents lists available at ScienceDirect

International Journal of Engineering Science

journal homepage: www.elsevier.com/locate/ijengsci

Full length article

Multi-scale non-affine mechanics of electro-magneto-active elastomers: Taut domain exploitable convolution of polymer chain crosslinks, entanglements and finite extensibility

Aman Khurana [a], Susmita Naskar [b], M.M. Joglekar [c], Tanmoy Mukhopadhyay [b,*]

[a] Department of Mechanical Engineering, Indian Institute of Technology Indore, Madhya Pradesh, 453552, India
[b] Faculty of Engineering and Physical Sciences, University of Southampton, Southampton, UK
[c] Department of Mechanical and Industrial Engineering, Indian Institute of Technology Roorkee, Uttarakhand, 247667, India

ARTICLE INFO

Keywords:
Smart electromagnetic thin membrane
Taut domains
Entanglements
Crosslinks
Finite extensibility
Non-affine model

ABSTRACT

Actuation devices fabricated using smart polymers often exhibit wrinkling and pull-in instability when they are subjected to external stimulation. These instabilities can disrupt the intended functionality of the actuation devices and hinder their reliability. The underlying reason for these instabilities is the complicated architecture of the polymer network, which results in a complex and chaotic arrangement of crosslinks and entanglements in smart elastomer membranes. This convoluted structure significantly influences the mechanical behavior of the polymers when external forces are applied. To better understand and characterize these instability phenomena, the present study develops a physics-based non-affine material model incorporating the effects of critical factors like polymer chain crosslinks, entanglements, and finite extensibility. By considering the intricate interplay among these factors, the model provides fundamental insights into the mechanisms behind the instability phenomena in smart polymers. Subsequently, the study explores the relationship between the applied electromagnetic field and the taut domains. The findings reveal that the size of the taut domains can be effectively altered by manipulating the levels of polymer chain crosslinks, entanglements, and finite extensibility. It is observed that, for a given level of applied electromagnetic field, increasing the entanglement and crosslink parameter leads to a larger taut domain. Conversely, an increase in the finite extensibility of the polymer chain diminishes the taut domain under the same level of electromagnetic loading. These understandings open up new avenues for optimizing actuation devices by adjusting the intricate properties of polymer chains to enhance stability and performance by unlocking the full multi-physical potential of smart elastomers.

1. Introduction

Smart electromagnetically active (EMA) polymers offer innovative and intelligent solutions for the advancement of next-generation robots, architected materials and actuation devices (Bandopadhya et al., 2007; Khurana et al., 2021b; Kundu et al., 2023; Machado et al., 2022; Patra et al., 2024; Sharma & Saxena, 2021; Singh et al., 2022a; Sinha & Mukhopadhyay, 2023; Yarali et al., 2022). These polymers possess remarkable attributes such as high deformability, lightweight nature, high energy density, and exceptional responsiveness to various stimuli, making them highly suitable for the burgeoning field of soft robotics. Soft robotic

* Corresponding author.
E-mail address: t.mukhopadhyay@soton.ac.uk (T. Mukhopadhyay).

https://doi.org/10.1016/j.ijengsci.2025.104378
Received 15 October 2024; Received in revised form 23 August 2025; Accepted 24 August 2025
Available online 16 September 2025

applications necessitate multiple input controls, including electrical, magnetic, and mechanical, where EMA polymers excel in meeting these requirements (Agrawal & Khurana, 2025; Agrawal et al., 2025; Khurana et al., 2021c; Moreno-Mateos et al., 2022; Patra et al., 2024). By incorporating multiple control modes into a single device, faster and more precise actuator control can be achieved, while simultaneously enabling high load-carrying capacity. Moreover, the integration of multiple input controls is crucial for the development of intelligent systems employed in contemporary applications such as surgical manipulators, energy harvesters and electromagnetic braking systems (Rabczuk et al., 2023; Sharma et al., 2025; Thai et al., 2023; Yarali et al., 2020).

EMA polymer-based actuators utilize a thin polymer sheet sandwiched between compliant electrodes, activated by an applied electromagnetic field source. This intelligent actuation method relies on inducing deformation through electromagnetic forces. The electro/magneto-thermal-mechanical deformation behavior of smart polymers, particularly electroactive and magnetoactive elastomers, has been extensively studied due to the complex coupling between multiple physical fields in these materials (Christensen et al., 2019; Kleo et al., 2020; Mehnert et al., 2021a, 2021b; Pandey et al., 2024). Unlike purely electro-or magneto-mechanically driven systems (Ghuku et al., 2025; Kundu et al., 2024; Mondal et al., 2025; Singh et al., 2022b; Sinha & Mukhopadhyay, 2023), real-world applications often involve significant thermal effects that influence material stiffness, actuation strain, and long-term stability. For instance, Zhao and Suo (2010) presented a thermodynamically consistent framework for dielectric elastomers that incorporates large deformation, electric field coupling, and temperature effects, highlighting the importance of thermal softening in the actuation process. Similarly, Kanan et al. (2024) developed a comprehensive model capturing the coupled electro-magneto-thermal-mechanical response of soft active materials, which is essential for accurately predicting performance under real operating conditions.

However, the failure mechanisms of such actuators are predominantly driven by sudden loss of equilibrium caused by in-plane compression. This is a well-established observation in the field of soft dielectric and magnetoactive elastomers, particularly those undergoing large deformations under combined electrostatic and magnetic loading. This phenomenon has been reported in experimental and theoretical studies (Chen et al., 2023; De Tommasi et al., 2010; Gour et al., 2025; Plante & Dubowsky, 2006) on dielectric elastomer actuators (DEAs) and magnetoactive membranes, where the application of an electric or magnetic field induces compressive in-plane stresses. When these stresses reach a critical threshold, they can lead to a snap-through instability, wrinkling, or even catastrophic collapse due to the loss of mechanical equilibrium. In this regard, only a handful of investigations have explored the initiation of deformation localizations based on electro-magneto-mechanical instability (Alameh et al., 2018; Kumar & Sarangi, 2018). In contrast, a series of articles and related studies have extensively investigated deformation localizations triggered by electro-mechanical instability (De Tommasi et al., 2011; Díaz-Calleja et al., 2008; He et al., 2009; Kumar et al., 2023; Pandey et al., 2023; Plante & Dubowsky, 2006). In the context of smart polymers based on EMA materials, the term “taut states” refers to the in-plane principal stretch responses obtained in smart actuator during activation, neglecting the bending stiffness of the smart membranes. However, the presence of bending stiffness in smart membranes leads to the buckling of thin films under compression, causing film distortion (De Tommasi et al., 2012; Steigmann & Pipkin, 1989). Taut states encompass regions with positive in-plane principal stretches (tensile configurations) or regions with a single positive principal stretch (wrinkled configurations) (Khurana et al., 2022). Conversely, regions with none of the principal stretches positive are referred to as bounded or balanced regions, where a sudden loss of equilibrium is not observed as in taut domains. Hence, the taut states are not feasible in these regions. Identifying these taut domains is crucial for determining the EMA material-based device design states. The presence and behavior of taut domains are critical in applications requiring controlled deformation and durability, as per the following explanations. (1) Stretchable Electronics and Soft Robotics: In flexible electronic substrates and soft robotic actuators, maintaining mechanical integrity under large deformations is essential. Taut domains influence the local modulus variations, helping engineers optimize material formulations to achieve a balance between flexibility and mechanical stability. (2) Wearable and Biomedical Devices: In applications such as bio-integrated electronics, prosthetics, and tissue engineering scaffolds, materials must sustain repeated mechanical loads without premature failure. Taut domain behavior can be leveraged to design materials with improved fatigue resistance and predictable stress–strain response. (3) Energy Absorbing and Protective Materials: Materials used in impact-resistant coatings, foams, and damping systems rely on controlled energy dissipation mechanisms. Taut domains contribute to strain localization and energy distribution, enabling tunable mechanical properties for shock absorption and vibration damping. As a broader implication, by characterizing taut domains, we can rationally tune polymer architectures (e.g., adjusting cross-link density, entanglement interactions, or filler reinforcement) to achieve desired mechanical responses. This understanding bridges molecular-scale interactions with macroscopic performance, providing a pathway for tailoring materials to specific application needs. In summary, the taut domain insights directly inform material selection and structural tuning for enhanced device functionality. With reference to past research on the taut domains, most studies have been dedicated to investigating the failure mechanisms associated with electric field-induced wrinkling in dielectric elastomeric-based actuators (De Tommasi et al., 2011; Khurana et al., 2022, 2022; Li et al., 2018; Shui et al., 2019).

Modeling the nonlinear mechanics of soft materials has been a longstanding challenge, with significant implications for designing smart elastomers. Puglisi and Saccomandi (2016) provided influential insights on multiscale approaches, emphasizing how molecular-level mechanisms such as chain extensibility and network structure directly inform macroscopic constitutive responses. Their work highlighted the importance of bridging scales when modeling soft tissues and elastomers, a perspective particularly relevant for EMA polymers where microstructural effects govern actuation efficiency and durability. Complementing this, Destrade et al. (2017) proposed a systematic framework for fitting constitutive models to experimental data. Their methodical approach improves predictive accuracy and reduces ambiguity in parameter identification, which is crucial when developing robust models for multifunctional polymer actuators operating under coupled electro-magneto-thermal fields. Puglisi and Saccomandi (2015) revisited the Gent model, demonstrating how its simplicity captures essential features of finite chain extensibility while remaining analytically

tractable. This balance between physical realism and mathematical elegance makes the Gent model a valuable tool for analyzing damage in thin elastomer membranes. Together, such studies provide a solid theoretical foundation that connects molecular-scale physics, constitutive modeling, and experimental calibration, directly informing the design and optimization of EMA polymer-based devices.

There exist numerous chain crosslinks and entanglements in the polymeric network of every soft material that is crucial in tuning the desirable properties of such smart polymers. Further, the polymer chains in smart elastomers have a limited length (Davidson & Goulbourne, 2013; Li et al., 2016), which imposes a termination point on the extension of the elastomers (Zhang et al., 2018). This finite extensibility of the polymer chains is a critical factor that influences the mechanical behavior of smart elastomers. The functionality of intelligent material-based soft actuators is significantly impacted by the entanglements, crosslinks, and finite extensibility of polymeric networks (Zhang et al., 2018; Zhu et al., 2018). Previous works, such as Davidson and Goulbourne's non-affine model (Davidson & Goulbourne, 2013), have provided a physics-based understanding of these effects in elastomeric materials undergoing finite deformations. Zhu and Luo (2017, 2018), Zhu et al. (2018) further interrogated the influence of entanglements and chain extensibility on the response of hydrogels, noting transformations in their mechanical behavior. Additionally, Zhu and Luo (2017), Zhu et al. (2018) presented an alternative non-affine model to analyze the chain entanglements impact on the electromechanical instability of dielectric elastomers under biaxial prestress. It was found that a higher degree of entanglement led to a lower critical actuation stretch and greater critical electric field (Khurana et al., 2021a; Zhang et al., 2018; Zhu & Luo, 2017). Moreover, it is observed that chain entanglements play a considerable role in these polymers' snap-through instability and failure path. Experimental studies have also shown that parameters such as crosslinking density, polymer chain entanglement, and finite extensibility significantly modulate the thermomechanical behavior, particularly under cyclic loading and elevated temperatures (Fan et al., 2001; Wang et al., 2022). These findings underscore the necessity of considering multi-physics interactions to fully understand and design high-performance electro- and magneto-responsive polymer actuators.

Motivated by previous research, the current investigation focuses on analyzing the influence of polymer chain entanglements, crosslinks, and finite extensibility on the behavior of smart membranes within the framework of taut domains. Specifically, we introduce such exploitable fundamental concepts to electro-magneto-active thin membranes, aiming to develop innovative smart actuator designs for advanced engineering applications. Our investigation aims to unveil the effects of inherently advantageous characteristics of smart membranes through the incorporation of taut domains and the coupling of electro-magneto-mechanical fields, which have not been previously investigated in the literature. The analytical findings of this article will contribute significantly to the existing literature in two major ways. First, to analyze the taut states of smart actuators, we develop a closed-form solution taking into account the electromagnetic field effect. Secondly, unlike previous models, our proposed approach takes into account the crucial effects of microcosmic properties inherent to smart elastomeric membranes.

The structure of the remaining article is conceptualized as follows. In Section 2, we propose an electro-magneto-mechanical model based on continuum mechanics that accounts for polymer chain crosslinks, entanglements, and finite extensibility. This model predicts the thresholds on the taut domains within the principal stretch plane of a smart membrane, considering the influence of polymer chain crosslinks, entanglements, and finite extensibility. Section 3, after model validation, presents a comprehensive computational study that thoroughly investigates how polymer chain internal properties alter the taut states of smart actuators excited by electromagnetic fields. This analysis provides fundamental insights into the behavior and characteristics of the taut domains. Finally, in Section 4, we summarize the significant findings of the study and discuss their implications, as well as outline potential avenues for future research.

2. Material modeling of smart thin membrane

The study focuses on electro-magneto-active elastomers, which exhibit significant deformation under applied electric and magnetic fields. To model their behavior, we use the thin membrane approximation, a common approach in the literature for materials with large deformation and flexible nature (Suo et al., 2008; Wissler & Mazza, 2005; Zhao & Suo, 2010). The use of the thin membrane model allows for tractable analysis of key phenomena such as electromechanical coupling and actuation behavior, which are essential for understanding the performance of electro-active elastomers in practical applications. It is important to note that while the modeling approach is simplified, it remains highly relevant to the electro-magneto-active elastomer systems under consideration. This simplified model effectively captures the essential electromechanical coupling and actuation behaviors, providing valuable insights into the engineering performance of these materials. Specifically, this section outlines the governing equations that characterize a smart thin membrane's behavior under electromagnetic loading. These equations are derived based on the theory of electro-magneto-elasticity, which has been developed and documented in literature (Agrawal & Khurana, 2025; Alblas, 1974; Bardzokas et al., 2007; Kumar & Sarangi, 2019a). This concept allows us to account for the inherent behavior and characteristics of the smart electro-magneto-elastic material class under consideration. Further, we derive the nonlinear expressions that describe the taut states within the smart actuator. These expressions capture the intricate relationship between the multi-physical external fields, the material properties of the membrane, and the resulting deformations.

2.1. Governing equation

We have considered a smart elastomeric membrane with polymer chain networks as illustrated in Fig. 1. The schematic highlights three key features of the polymer network, as shown in Fig. 1(a): 1. Entanglements (illustrated by intertwined dark blue and light green curves) depict physical, non-covalent constraints that restrict the movement of chains due to topological interlocking,

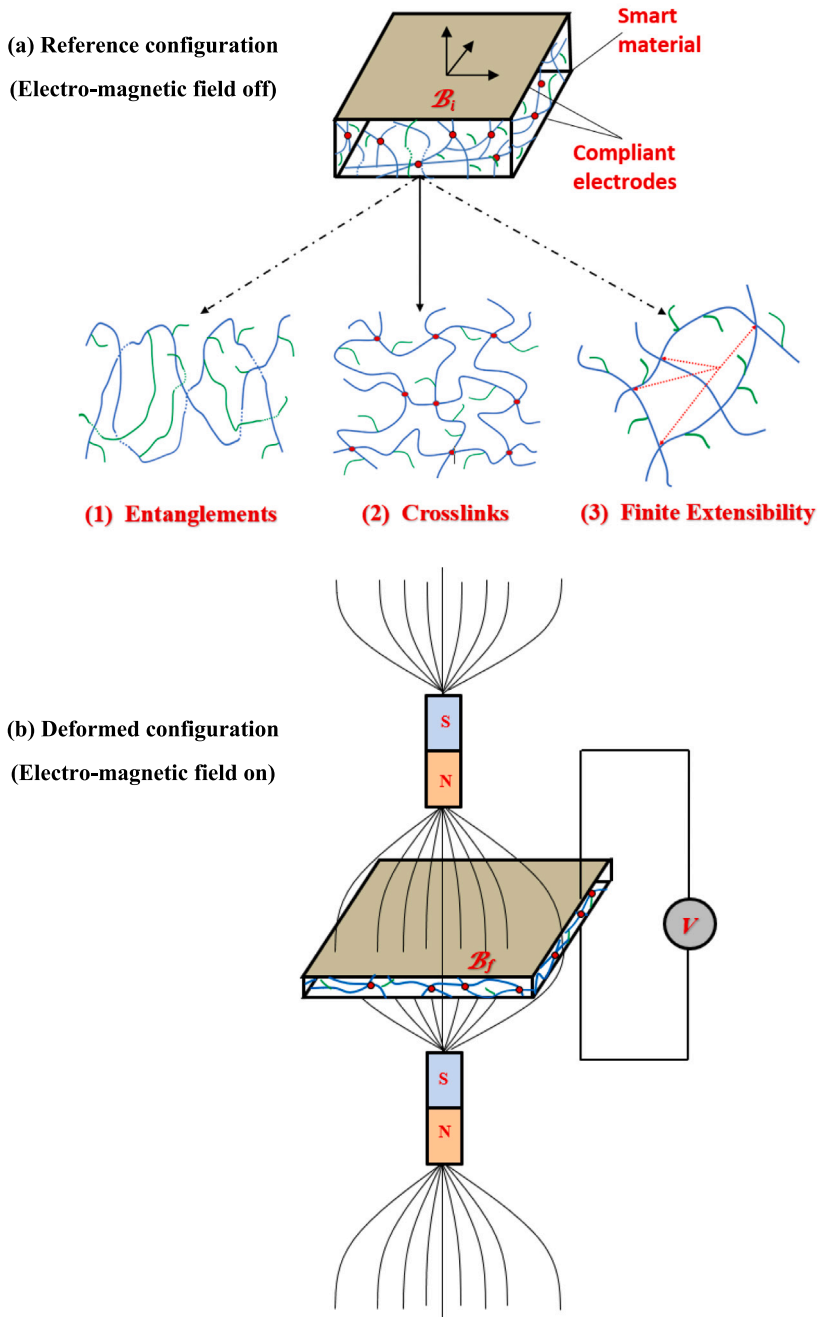

Fig. 1. A schematic depiction of smart membranes exhibiting entanglement, crosslinks, and the finite extensibility of polymer chains in both (a) its reference configuration, and (b) its deformed configuration under electromagnetic loading.

contributing to the material's elasticity and viscoelastic behavior, 2. Crosslinks (denoted by red filled circles) represent permanent covalent bonds that anchor the polymer chains and provide structural integrity to the elastomer network, and 3. Finite extensibility (indicated by red dashed boundaries) shows the maximum possible extension of individual polymer chains, beyond which the chains can no longer stretch, leading to pronounced non-linear stiffening in the elastomer's macroscopic response.

In the context of a developed smart elastomeric membrane, we consider a reference state denoted as $\mathcal{B}_i$, as depicted in Fig. 1(a). The membrane undergoes deformation when excited by an applied electromagnetic field, resulting in a current configuration denoted as $\mathcal{B}_f$ (Fig. 1(b)). The deformation is represented by a deformation gradient $\mathbf{F} = \nabla\mathbf{f}$, where $\mathbf{f}$ is the mapping from the reference configuration to the current configuration. The expression of the left Cauchy–Green deformation tensor $\mathbf{B}$ for the specified

deformation $\mathbf{F}$ is expressed as $\mathbf{B} = \mathbf{F}\mathbf{F}^T$. The tensor $\mathbf{B}$ can be written as a summation over the three principal stretches, λ_i, along the principal directions $\mathbf{e}_i$, i.e., $\mathbf{B} = \sum_{i=1}^{3} \lambda_i^2 \mathbf{e}_i \otimes \mathbf{e}_i$. In the present arrangement, the electromagnetic field variables are designated as $\mathbf{E}$ and $\mathbf{H}$, symbolizing the electric and magnetic fields, respectively. These variables characterize the electromagnetic properties of the membrane during deformation.

For a smart electro-magneto-elastic membrane, let us assume that the free energy density is denoted as Ω and is a function of the deformation gradient tensor $\mathbf{F}$, the electric field vector $\mathbf{E}$, and the magnetic field vector $\mathbf{H}$ as $\Omega = \Omega(\mathbf{F}, \mathbf{E}, \mathbf{H})$. In the framework of the coupled nonlinear theory of electro-magneto-elasticity, the total stress tensor $\mathbf{T}$ of an incompressible smart material system can be articulated as (Kumar & Sarangi, 2019a):

$$\mathbf{T} = -p\mathbf{I} + \lambda_i \left(\frac{\partial \Omega}{\partial \lambda_i} \right), \tag{1}$$

where, in the context of the incompressible smart electro-magneto-elastic membrane, the Lagrange multiplier, denoted as p, is introduced to enforce the incompressibility constraint. This constraint ensures that the volume of the membrane remains constant during deformation. In the specific membrane configuration illustrated in Fig. 1, the deformation gradient tensor $\mathbf{F}$, the left Cauchy–Green deformation tensor $\mathbf{B}$, the electric and the magnetic field vector $\mathbf{E}$ and $\mathbf{H}$ are articulated as follows:

$$\mathbf{F} = \lambda_1 \mathbf{e}_1 \otimes \mathbf{E}_1 + \lambda_2 \mathbf{e}_2 \otimes \mathbf{E}_2 + \lambda_1^{-1}\lambda_2^{-1} \mathbf{e}_3 \otimes \mathbf{E}_3, \quad \mathbf{B} = \mathbf{F}\mathbf{F}^T, \quad \mathbf{E} = E_0 \mathbf{e}_3, \quad \mathbf{H} = H_0 \mathbf{e}_3, \tag{2}$$

In the given problem, the basis vectors $\mathbf{E}_1$, $\mathbf{E}_2$, $\mathbf{E}_3$ represent the basis in the reference configuration of the membrane, while the basis vectors $\mathbf{e}_1$, $\mathbf{e}_2$, $\mathbf{e}_3$ represent the basis in the current configuration. These basis vectors define the coordinate systems in the respective configurations. The corresponding free energy density expression for a soft polymeric film using a physics-based non-affine type of material model is given by Davidson and Goulbourne (2013)

$$\Omega_{strain} = \begin{bmatrix} \frac{1}{6}\mu_c \left(\lambda_1^2 + \lambda_2^2 + \lambda_3^2 \right) \\ -\mu_c \lambda_{\max}^2 \ln\left(3\lambda_{\max}^2 - \lambda_1^2 - \lambda_2^2 - \lambda_3^2 \right) \\ +\mu_e \left(\lambda_1 + \lambda_2 + \lambda_3 + \lambda_1^{-1} + \lambda_2^{-1} + \lambda_3^{-1} \right) \end{bmatrix}, \tag{3}$$

where μ_c represents the network modulus describing the stiffness of the cross-linked network within the polymer indicating how resistant the material is to deformation, λ_{max} signifies the maximum extent to which the polymer chains can be stretched or elongated before reaching their limit of extension, and μ_e is the entanglement modulus that characterizes the resistance of the polymer chains to sliding or disentangling, affecting the material's overall mechanical behavior.

The expression for the work done by external electrostatic and magnetic forces is written as:

$$\Omega_{ext} = -\left[\underbrace{\left(\frac{1}{2}\varepsilon_0 E_0^2 \lambda_1^2 \lambda_2^2 \right)}_{electrical} + \underbrace{\left(\frac{1}{2}\alpha_0 H_0^2 \lambda_1^{-2} \lambda_2^{-2} \right)}_{magnetic} \right], \tag{4}$$

where ε_0 and α_0 represents the electric permittivity and the magnetic permeability of the smart membrane, respectively. The electro-magneto-mechanical free energy in this study is formulated in a general form to capture the coupled field-induced deformations in electro-magneto-active elastomers (EMMEs) (Behera et al., 2023; Zhang et al.). These materials consist of dielectric polymer networks embedded with magnetic particles, enabling simultaneous electro-and magneto-mechanical responses. The formulation accounts for the interplay between electric and magnetic field effects through the mechanically coupled polymer matrix, allowing for a unified treatment of complex multi-field interactions in non-affine, extensible networks. By considering different contributions (as presented in Eqs. (3)–(4)), the total free energy density Ω provides a comprehensive description of the energy stored within the smart actuator, taking into account its isotropic behavior as well as the effects of electrostatic and magnetic interactions, and is written as:

$$\Omega = \underbrace{\begin{bmatrix} \frac{1}{6}\mu_c \left(\lambda_1^2 + \lambda_2^2 + \lambda_3^2 \right) \\ -\mu_c \lambda_{\max}^2 \ln\left(3\lambda_{\max}^2 - \lambda_1^2 - \lambda_2^2 - \lambda_3^2 \right) \\ +\mu_e \left(\lambda_1 + \lambda_2 + \lambda_3 + \lambda_1^{-1} + \lambda_2^{-1} + \lambda_3^{-1} \right) \end{bmatrix}}_{strain} - \left[\underbrace{\left(\frac{1}{2}\varepsilon_0 E_0^2 \lambda_1^2 \lambda_2^2 \right)}_{electrical} + \underbrace{\left(\frac{1}{2}\alpha_0 H_0^2 \lambda_1^{-2} \lambda_2^{-2} \right)}_{magnetic} \right]. \tag{5}$$

In the present work, we have not explicitly included deformation gradient terms in our free energy density as incorporated by Zurlo et al. (2017). The current approach provides a different but complementary perspective on the behavior of elastomers, particularly under magneto-electro-mechanical coupling. The presence of taut domains in our formulation helps capture key nonlinear deformation characteristics, which indirectly relate to thinning effects. We note that incorporating deformation gradient terms, as demonstrated by Zurlo et al. (2017), could enhance the predictive accuracy regarding failure mechanisms in smart elastomers. Future work could extend our model by introducing higher-order deformation terms to analyze whether similar catastrophic thinning behaviors arise under coupled electro-magnetic loading conditions.

By substituting the expression of the total free energy density (Eq. (5)) into the definition of the total stress tensor (Eq. (1)), the principal stress components of the smart membrane in the deformed configuration can be determined as follows:

$$\begin{aligned} T_{11} &= -p + \frac{\mu_c}{3}\lambda_1^2 + \frac{2\mu_c\lambda_{\max}^2\lambda_1^2}{\left(3\lambda_{\max}^2 - \lambda_1^2 - \lambda_2^2 - \lambda_3^2\right)} + \mu_e\left(\lambda_1 - \lambda_1^{-1}\right) - \varepsilon_0 E_0^2\lambda_1^2\lambda_2^2 + \alpha_0 H_0^2\lambda_1^{-2}\lambda_2^{-2}, \\ T_{22} &= -p + \frac{\mu_c}{3}\lambda_2^2 + \frac{2\mu_c\lambda_{\max}^2\lambda_2^2}{\left(3\lambda_{\max}^2 - \lambda_1^2 - \lambda_2^2 - \lambda_3^2\right)} + \mu_e\left(\lambda_2 - \lambda_2^{-1}\right) - \varepsilon_0 E_0^2\lambda_1^2\lambda_2^2 + \alpha_0 H_0^2\lambda_1^{-2}\lambda_2^{-2}, \\ T_{33} &= -p + \frac{\mu_c}{3}\lambda_3^2 + \frac{2\mu_c\lambda_{\max}^2\lambda_3^2}{\left(3\lambda_{\max}^2 - \lambda_1^2 - \lambda_2^2 - \lambda_3^2\right)} + \mu_e\left(\lambda_3 - \lambda_3^{-1}\right). \end{aligned} \tag{6}$$

When the stress-free state boundary condition ($T_{33} = 0$) is applied in the above equation (Eq. (6)), the Lagrange multiplier p is obtained as follows:

$$T_{33} = 0 \Rightarrow p = \frac{\mu_c}{3}\lambda_3^2 + \frac{2\mu_c\lambda_{\max}^2\lambda_3^2}{\left(3\lambda_{\max}^2 - \lambda_1^2 - \lambda_2^2 - \lambda_3^2\right)} + \mu_e\left(\lambda_3 - \lambda_3^{-1}\right). \tag{7}$$

The principal stress components (T_{11} and T_{22}) can be derived by invoking the deduced expression of the Lagrange multiplier p into the Eq. (6) as

$$\begin{aligned} T_{11} &= \mu_c\left(\lambda_1^2 - \lambda_3^2\right)\left\{\frac{1}{3} + \frac{2\lambda_{\max}^2}{\left(3\lambda_{\max}^2 - \lambda_1^2 - \lambda_2^2 - \lambda_3^2\right)}\right\} + \mu_e\left(\lambda_1 - \lambda_1^{-1} - \lambda_3 + \lambda_3^{-1}\right) - \varepsilon_0 E_0^2\lambda_1^2\lambda_2^2 + \alpha_0 H_0^2\lambda_1^{-2}\lambda_2^{-2}, \\ T_{22} &= \mu_c\left(\lambda_2^2 - \lambda_3^2\right)\left\{\frac{1}{3} + \frac{2\lambda_{\max}^2}{\left(3\lambda_{\max}^2 - \lambda_1^2 - \lambda_2^2 - \lambda_3^2\right)}\right\} + \mu_e\left(\lambda_2 - \lambda_2^{-1} - \lambda_3 + \lambda_3^{-1}\right) - \varepsilon_0 E_0^2\lambda_1^2\lambda_2^2 + \alpha_0 H_0^2\lambda_1^{-2}\lambda_2^{-2}. \end{aligned} \tag{8}$$

Taking into account the incompressible nature of the smart membrane, i.e., $\lambda_1\lambda_2\lambda_3 = 1$, the expressions for the principal stress components can be rephrased as follows:

$$\begin{aligned} T_{11} &= \mu_c\left(\lambda_1^2 - \lambda_1^{-2}\lambda_2^{-2}\right)\left\{\frac{1}{3} + \frac{2\lambda_{\max}^2}{\left(3\lambda_{\max}^2 - \lambda_1^2 - \lambda_2^2 - \lambda_1^{-2}\lambda_2^{-2}\right)}\right\} + \mu_e\left(\lambda_1 - \lambda_1^{-1} - \lambda_1^{-1}\lambda_2^{-1} + \lambda_1\lambda_2\right) - \varepsilon_0 E_0^2\lambda_1^2\lambda_2^2 + \alpha_0 H_0^2\lambda_1^{-2}\lambda_2^{-2}, \\ T_{22} &= \mu_c\left(\lambda_2^2 - \lambda_1^{-2}\lambda_2^{-2}\right)\left\{\frac{1}{3} + \frac{2\lambda_{\max}^2}{\left(3\lambda_{\max}^2 - \lambda_1^2 - \lambda_2^2 - \lambda_1^{-2}\lambda_2^{-2}\right)}\right\} + \mu_e\left(\lambda_2 - \lambda_2^{-1} - \lambda_1^{-1}\lambda_2^{-1} + \lambda_1\lambda_2\right) - \varepsilon_0 E_0^2\lambda_1^2\lambda_2^2 + \alpha_0 H_0^2\lambda_1^{-2}\lambda_2^{-2}. \end{aligned} \tag{9}$$

The expression of first Piola–Kirchhoff (PK-1) stress components S_{ii} can be obtained from the derived principal stress components (Eq. (6)) using the following conversion formula:

$$S_{ii}(\lambda_1, \lambda_2, E_0, H_0) = \mathrm{T}_{ii}(\lambda_1, \lambda_2, E_0, H_0)\lambda_{\mathrm{i}}^{-1}, \qquad i = 1, 2. \tag{10}$$

The subsequent subsection introduces the taut states framework, which plays a critical role in capturing the essential kinematic constraints and non-affine deformation characteristics of the membrane. This framework provides the foundation for linking the macroscopic behavior with the underlying microstructural mechanics central to our multi-scale model.

2.2. Taut states framework

This subsection explores the idea of the taut state (refer to Fig. 2), also referred to as the tensile stretches region (Steigmann & Pipkin, 1989), for the developed smart thin membrane. The membrane is presumed to have a uniform thickness and a cylindrical shape in its flat mid-surface, as illustrated by reference configuration $\mathcal{B}_i$ in Fig. 1(a). Throughout the loading process, the membrane remains flat, disregarding any orthogonal displacements of the corresponding mid-surface.

To establish the constitutive relations for taut domains in a smart electro-magneto-active thin membrane, we consider a local uniaxial stress applied in the direction of $\mathbf{e}_2$. Notably, under the condition where $T_{11} = T_{33} = 0$ for uniaxial stress, a unique value is assumed by the transverse stretch in the $\mathbf{e}_1$ direction, referred to as the natural width in tension. Taking this condition into account, the taut domains presented in Eq. (9)(a) are reformulated as follows:

$$\mu_c\left(\lambda_1^2 - \lambda_1^{-2}\lambda_2^{-2}\right)\left\{\frac{1}{3} + \frac{2\lambda_{\max}^2}{\left(3\lambda_{\max}^2 - \lambda_1^2 - \lambda_2^2 - \lambda_1^{-2}\lambda_2^{-2}\right)}\right\} + \mu_e\left(\lambda_1 - \lambda_1^{-1} - \lambda_1^{-1}\lambda_2^{-1} + \lambda_1\lambda_2\right) - \varepsilon_0 E_0^2\lambda_1^2\lambda_2^2 + \alpha_0 H_0^2\lambda_1^{-2}\lambda_2^{-2} = 0. \tag{11}$$

When dealing with a simple boundary value problem, we examine a smart thin membrane that exhibits zero tractions, activated by an electromagnetic field applied to both the upper and lower surfaces. By considering equibiaxial equilibrium configurations, where $\lambda_1 = \lambda_2 = \lambda$, we derive the required expressions for the Piola–Kirchhoff stress components using Eq. (10) as

$$\begin{aligned} S_{11}(\lambda, E_0, H_0) = S_{22}(\lambda, E_0, H_0) = S(\lambda, E_0, H_0) = \mu_c(\lambda - \lambda^{-5})\left\{\frac{1}{3} + \frac{2\lambda_{\max}^2}{\left(3\lambda_{\max}^2 - \lambda_1^2 - \lambda_2^2 - \lambda_1^{-2}\lambda_2^{-2}\right)}\right\} \\ + \mu_e\left(1 - \lambda^{-2} - \lambda^{-3} + \lambda\right) - \varepsilon_0 E_0^2\lambda^3 + \alpha_0 H_0^2\lambda^{-5}. \end{aligned} \tag{12}$$

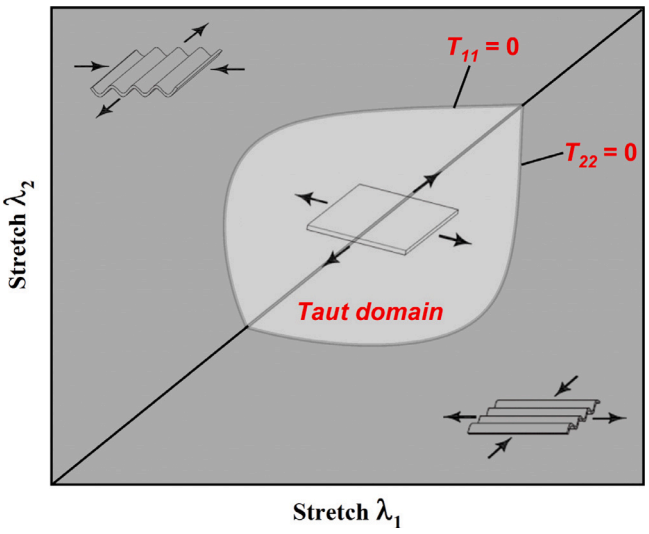

Fig. 2. A generalized taut domain curve for smart thin elastomeric membranes.

Furthermore, the equibiaxial stretch parameter λ aligns with the condition of null tractions along the edges of the membrane. This equibiaxial stretch is linked to the following solution:

$$S(\lambda, E_0, H_0) = 0,$$
$$\varepsilon_0 E_0^2 \lambda^8 - \alpha_0 H_0^2 - \mu_c(\lambda^6 - 1)\left\{\frac{1}{3} + \frac{2\lambda_{\max}^2}{\left(3\lambda_{\max}^2 - \lambda_1^2 - \lambda_2^2 - \lambda_1^{-2}\lambda_2^{-2}\right)}\right\} - \mu_e\left(\lambda^5 - \lambda^3 - \lambda^2 + \lambda^6\right) = 0. \tag{13}$$

The expression for the stability criterion necessary to achieve taut domains under homogeneous equibiaxial deformation is as follows:

$$\frac{dS(\lambda, \lambda)}{d\lambda} > 0. \tag{14}$$

In the impending section, the governing equation (Eq. (11)) is normalized and solved numerically for investigating the influence of smart thin membrane entanglements, crosslinks, and finite extensibility on the taut states resulting from applied electromagnetic actuation.

3. Results and analysis

In this section, we utilize the electro-magneto-mechanical model presented in Section 2 to make predictions about the thresholds on the taut domains within the principal stretches plane. First, the model's validity is established through comparisons with experimental investigation and the energy-based model proposed by Sharma and Joglekar (2018) on an isotropic smart dielectric elastomeric thin membrane, without a magnetic load ($h = 0$), under different levels of electrical loading conditions. Further, the impacts of polymer chain entanglements, crosslinks, and finite extensibility parameters on the taut domains are analyzed under electromagnetic field loading conditions.

3.1. Validation of the proposed taut domain framework

First, to validate the proposed framework under electrical actuation, a series of experiments are carried out using a widely accessible acrylic elastomeric membrane (VHB 4905) with shear modulus $\mu = 26.28$ kPa, thickness $t_0 = 0.5$ mm, and permittivity $\varepsilon_0 = 4.1595 \times 10^{-11}$ F/m (Khurana et al., 2022). The experimental methodology used to analyze the electromechanical behavior of the dielectric elastomer is illustrated schematically in Fig. 3(a). The DE membrane is affixed to a stretching mechanism, with a rigid PLA frame attached to both the top and bottom surfaces of the elastomer. Using carbon grease (MG chemicals, 846-80G), compliant electrodes are impregnated to the upper and bottom surfaces of the membrane. Copper strips are then utilized to connect the electrodes to the input voltage terminals. For the experimental characterization of the taut state behavior, a high voltage amplifier (Trek-610E) is employed, as illustrated in Fig. 3(b). In this study, we employed a commercially available acrylic membrane (VHB-4905), which is well known for its pronounced viscoelastic behavior (Huang et al., 2024; Khurana et al., 2021; Qin et al., 2023) - distinct from the purely hyperelastic assumptions underlying our analytical model. To minimize the influence of time-dependent effects and align the experimental conditions with the model's quasi-static framework, the membrane was first pre-stretched and subjected to a 24-hour stress relaxation period, allowing it to stabilize near equilibrium. Following this, a potential difference was applied at a controlled rate of 50 V/s using a high-voltage amplifier (Trek- 610E), ensuring gradual, quasi-static loading and reducing

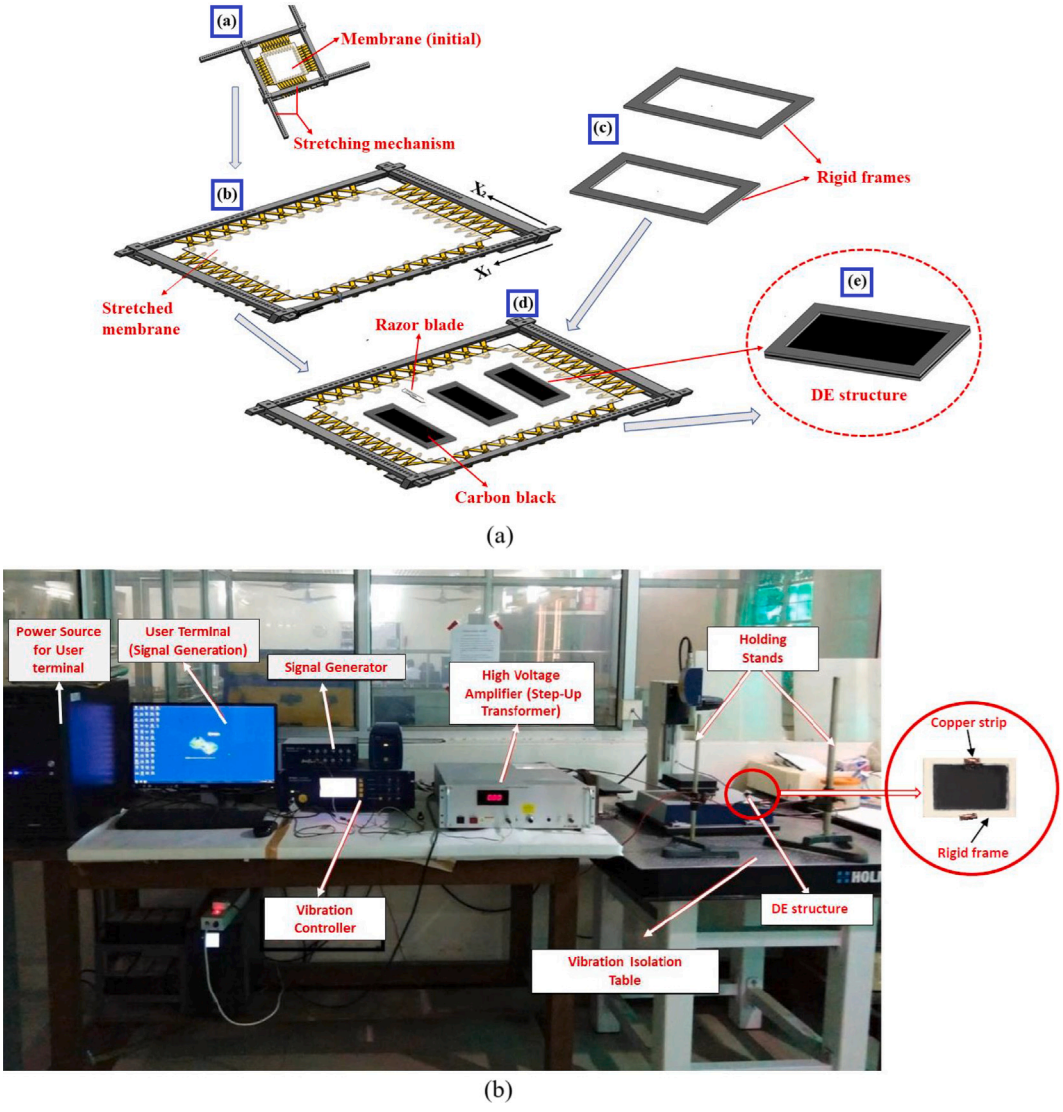

Fig. 3. (a) Experimental fabrication process of dielectric elastomer-based specimen, (b) Setup for analyzing the electromechanical behavior of the developed specimen.

the impact of viscoelasticity during actuation. When a dimensionless electric field $e = E_0\sqrt{\frac{\varepsilon_0}{\mu}} = \frac{\phi}{t_0}\sqrt{\frac{\varepsilon_0}{\mu}}$ is introduced, the observed subsequent events are shown in Fig. 4(a): initially, the membrane remains at rest, when no electric field is applied, $e = 0$. The membrane remains in a stable taut state, when the electric field is slowly increased. In the end, at $e = 0.69$, the membrane exhibits irreversible thinning. Following this catastrophic occurrence, the electrical breakdown of the membrane occurs and it becomes unusable.

Subsequently, we have implemented the same sets of material parameters in the developed taut domain framework (Eq. (11)) as considered for the experimental characterizations, i.e., shear modulus $\mu = \mu_e + \mu_c = 26.28$ kPa, thickness $t_0 = 0.5$ mm and permittivity $\varepsilon_0 = 4.1595 \times 10^{-11}$ F/m. The other considered parameters are $\frac{\mu_e}{\mu_c} = 0.10$, limiting stretch material constant $J_{\text{lim}} = 120$, and $\lambda_{\text{max}} = \sqrt{\frac{J_{\text{lim}}+3}{3}} \approx 6.4$ (Khurana et al., 2021a). The constitutive parameters used in this study are selected based on physically representative values reported in literature for similar elastomeric systems. While exact values for these parameters may not be directly available for the specific material considered, the model aims to provide a predictive framework that captures the essential multi-scale mechanics. Future experimental work, such as biaxial testing or dynamic mechanical analysis, can be used to calibrate these parameters for specific materials. It is observed from Fig. 4(b) that there exists a stable taut domain when applied electric field is in the range of 0.55–0.65. The taut area contracts as e increases, i.e., as the electrical potential increases, before the point of critical activation e_{crit} is attained. When the critical electric field value (e_{crit}) reaches 0.695, the taut region of an isotropic dielectric elastomer membrane becomes infinitesimally small (a single point), leading to a phenomenon known as Pull-in

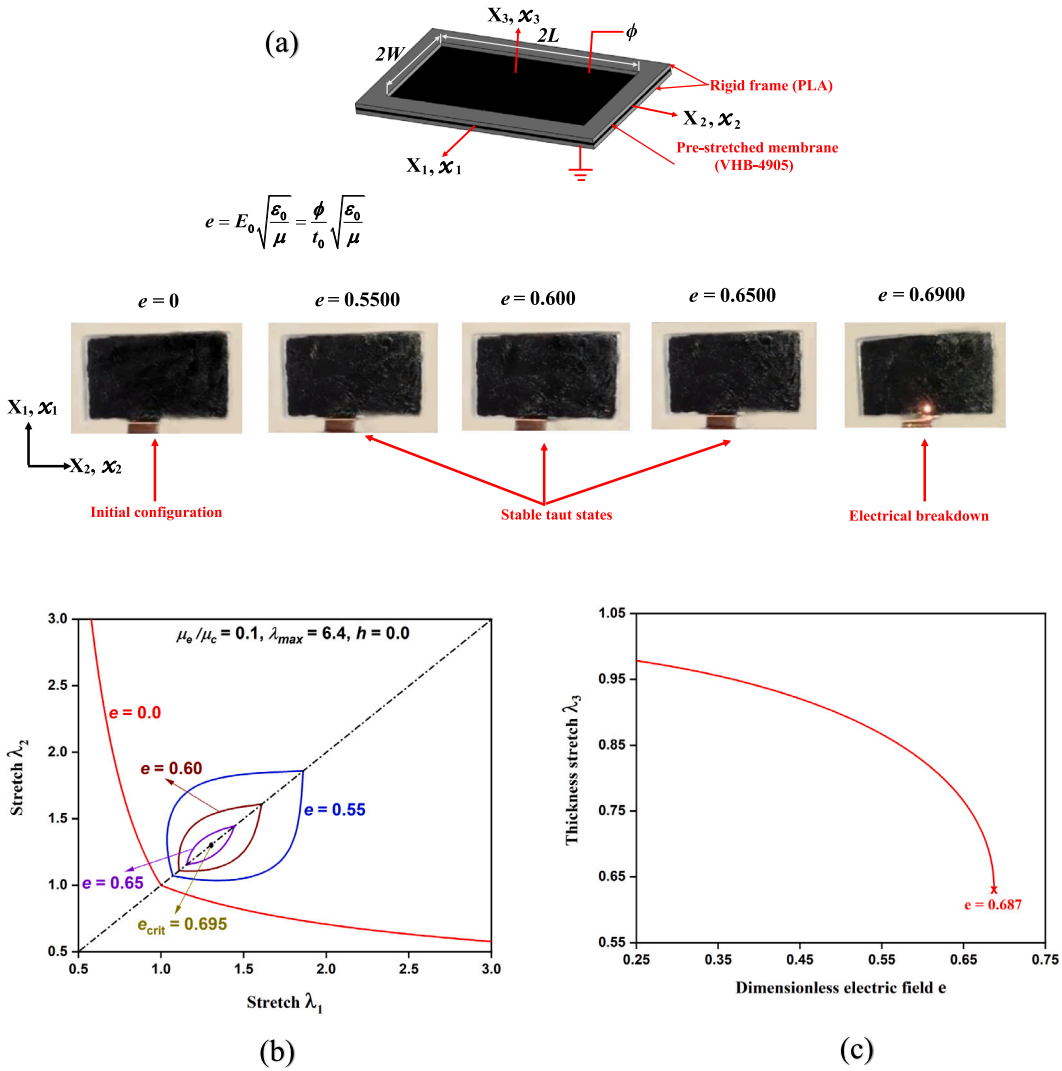

Fig. 4. A comparative perspective depicting the (a) experimental, (b) taut domains, and (c) energy-based characterization of smart elastomers obtained under different levels of electric field e (Sharma & Joglekar, 2018) ($h = 0$).

instability (Blok & LeGrand, 1969; Díaz-Calleja et al., 2008). As shown in Fig. 4(b), in the absence of an electric field, two asymptotes emerge from the point $(\lambda_1, \lambda_2) = (1,1)$, extending along the positive λ_1 and λ_2 axes. These asymptotes essentially represent what we refer to as "natural widths" (De Tommasi et al., 2012). This refers to the inherent contraction that occurs perpendicular to the direction of applied stretch in thin membranes. For instance, if the membrane is stretched along the X_1 direction, it naturally contracts along X_2 - the extent of which is marked by the asymptote extending along the λ_1 axis. When the transverse stretch λ_2 is below this natural width, the membrane enters a wrinkled state (see Fig. 2 for orientation). When λ_2 exceeds this threshold, the membrane remains taut. A similar interpretation holds for the asymptote along the X_2 direction. A key outcome of our analysis is that these natural width boundaries are not fixed; they evolve with the application of an electric field. As the field increases, the asymptotes form a closed region of taut states (Figs. 2 and 4(b)), which progressively shrinks and ultimately collapses to a point corresponding to electromechanical instability. This novel field-dependent evolution of the taut region is central to our study, where we examine the influence of various parameters (material-and actuation-related) on its shape and size. Highlighting the role of natural width in enabling control over membrane stability, the notion of natural width can also be extended to demarcate stable and unstable wrinkling regimes (as explored in our previous work Khurana et al., 2022). However, that specific analysis is beyond the scope of the present study. Here, our focus remains examining the influence of material and loading parameters on the onset of electro-magneto-mechanical instabilities.

In addition to the taut domain framework, researchers have previously utilized an energy-based method to analyze electromechanical instabilities, such as the Pull-in instability in dielectric membranes. Further, to determine the taut domain model's prediction

capabilities, we have employed an energy-based framework proposed by Sharma and Joglekar (2018). By incorporating the energy-based model, we have generated a plot depicting the relationship between thickness stretch and dimensionless electric field for a thin isotropic dielectric elastomer membrane (Fig. 4(c)). Subsequently, we have determined the critical electric field to be $e = 0.687$ for the isotropic dielectric elastomer actuator, indicated by the X symbol in Fig. 4(c).

In summary, a comprehensive comparative analysis has been performed here between the developed taut domain model and experimental results. Further, to determine the taut domain model's prediction capabilities, we have employed an energy-based framework proposed by Sharma and Joglekar (2018). From the discussion presented in this section, we conclude that the proposed taut domain framework accurately predicts the critical electric field required for the onset of pull-in instability in an isotropic actuator. This prediction aligns well with the critical electric field obtained from both experimental investigation and the energy-based computational framework. These findings verify the established model's accuracy in forecasting taut domains of the smart membrane within the principal stretches plane. In this context, we would like to mention that the main focus and contribution of this paper is computational model development. While Section 3.1 does not present discrete experimental data points in the form of traditional plots, the section indeed describes an experimental investigation aimed at qualitatively validating the theoretical predictions obtained from the taut domain analysis. Therefore, the experimental "campaign" here serves to qualitatively verify the absence of wrinkling and the taut behavior of the membrane under the specified conditions, rather than to provide a dense set of quantitative data points.

Despite the validations presented here, we acknowledge that a more comprehensive experimental validation can be performed in the future to firmly establish the generalizability and accuracy of the framework. As such, the following systematic experimental investigations (out of scope for the current paper) can be performed: (1) Quantitative comparison with stress–strain and displacement field data, (2) High-resolution imaging of taut domain evolution, and (3) Real-time electro-mechanical response under controlled field conditions. Such future studies will serve to strengthen the connection between the proposed theoretical model and physical observations, thereby enhancing confidence in its applicability to advanced smart elastomer-based actuators and sensors.

3.2. Effect of polymer chain entanglements

This subsection presents a methodology that utilizes the developed model to determine the thresholds of the taut states within the principal stretches plane of the smart membrane, considering different levels of polymer chain entanglements. In this methodology, we consider a constant density of crosslinks ($\mu_c = 1$) and investigate five different levels of dimensionless entanglement parameter $\mu_e/\mu_c = 0.0$, 0.25, 0.5, 0.75, and 1.0 (Davidson & Goulbourne, 2013; Zhu & Luo, 2017, 2018; Zhu et al., 2018). The extensibility parameter λ_{max} is set to 5 for all cases. To facilitate the analysis, we normalize Eqs. (11)–(12) with respect to μ_c and introduce dimensionless electromagnetic fields as follows:

$$e = E_0\sqrt{\frac{\epsilon_0}{\mu_c}}, \quad h = H_0\sqrt{\frac{\alpha_0}{\mu_c}}. \tag{15}$$

By employing these dimensionless fields, we can study the influence of entanglements on taut domains across various levels of entanglement parameters. This methodology allows us to explore the behavior and thresholds of taut states within the principal stretches plane under different polymer chain entanglement conditions. By inserting the normalized expressions of the magnetic and electric field variables into the governing Eqs. (11)–(12), the following set of normalized equations are obtained:

$$\left(\lambda_1^2 - \lambda_1^{-2}\lambda_2^{-2}\right)\left\{\frac{1}{3} + \frac{2\lambda_{\max}^2}{\left(3\lambda_{\max}^2 - \lambda_1^2 - \lambda_2^2 - \lambda_1^{-2}\lambda_2^{-2}\right)}\right\} + \frac{\mu_e}{\mu_c}\left(\lambda_1 - \lambda_1^{-1} - \lambda_1^{-1}\lambda_2^{-1} + \lambda_1\lambda_2\right) - e^2\lambda_1^2\lambda_2^2 + h^2\lambda_1^{-2}\lambda_2^{-2} = 0, \tag{16}$$

$$\begin{aligned} S_{11}(\lambda, e, h) = S_{22}(\lambda, e, h) = S(\lambda, e, h) = (\lambda - \lambda^{-5})&\left\{\frac{1}{3} + \frac{2\lambda_{\max}^2}{\left(3\lambda_{\max}^2 - \lambda_1^2 - \lambda_2^2 - \lambda_1^{-2}\lambda_2^{-2}\right)}\right\} \\ &+ \frac{\mu_e}{\mu_c}\left(1 - \lambda^{-2} - \lambda^{-3} + \lambda\right) - e^2\lambda^3 + h^2\lambda^{-5}. \end{aligned} \tag{17}$$

First, we analyze the taut state of the smart elastomer under different entanglement parameters (see Fig. 5), while maintaining a consistent applied electromagnetic field level ($e = h = 0.75$). The plot clearly illustrates that as the entanglement parameter decreases, the taut region of the membrane shrinks. This observation suggests that materials with higher levels of polymer chain entanglement exhibit a greater tensile stretch region. Also, the increase in the taut region with higher entanglement parameters indicates that the entanglement of polymer chains contributes to the increased stiffness and modulus of the elastomer material (Zhang et al., 2018). This, in turn, increases the elastomer's ability to stretch laterally. The phenomenon is beneficial when aiming to achieve a higher stretch at the point of instability.

Figs. 6(a, c, e) depict the taut state of the smart elastomer under three different entanglement parameters ($\mu_e/\mu_c = 0.0$, 0.5, and 1.0) for various levels of applied electric field. The magnetic field is kept constant at $h = 0.75$. In all the cases considered, the taut region diminishes as the applied electric field (e) is increased, until a critical activation point (e_{crit}) is reached. The taut region of the smart elastomer reduces to a single point at $e_{crit} = 0.795$, 0.935, and 1.075 for entanglement parameters $\mu_e/\mu_c = 0.0$, 0.5, and 1.0, respectively. This behavior suggests that as the voltage increases, more entangled smart polymers require a higher electric field for their breakdown. The model captures this by demonstrating that at a critical electric field level (e_{crit}), the taut domain shrinks to a point, beyond which the material cannot support tensile stresses due to excessive electrostatic compression. This transition point is observed at progressively higher electric fields for more entangled polymer networks, indicating that materials

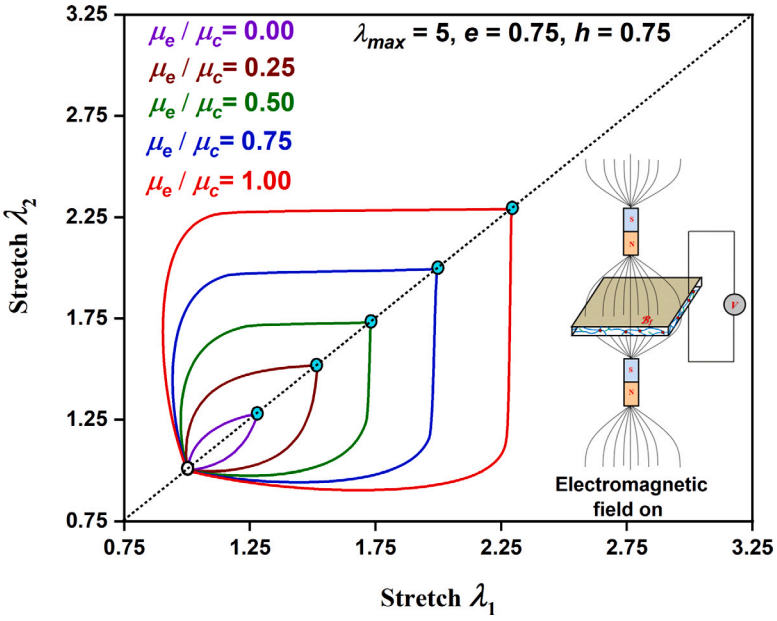

Fig. 5. Taut state curves of a smart elastomer for different entanglement parameter (μ_e/μ_c) subjected to an electromagnetic field (e = 0.75, h = 0.75) with λ_{max} = 5.

with greater entanglement (i.e., higher effective stiffness) resist this softening longer. It is worth noting that at higher voltages, there are no taut states observed in any of the cases. Interestingly, a higher electric field (e) corresponds to a lower effective stiffness of the membrane (Wissler & Mazza, 2007; Zhao & Suo, 2010). Consequently, it can be inferred that materials with higher stiffness demonstrate an expanded region of tensile stretch (De Tommasi et al., 2012). Similarly, Figs. 6(b, d, f) illustrate the stretched conditions of the smart membrane at different magnetic field intensities, while keeping the applied electric field constant (e = 0.75). In contrast to the previous scenario, the taut regions of the smart elastomer expand as the applied magnetic loading increases for all the considered levels of polymer chain entanglements, demonstrating an advantageous impact on the taut behavior. This expansion suggests that magnetic loading enhances the effective stiffness, likely through magneto-mechanical interactions that induce localized tension. The numerical model incorporates these magnetic effects via body forces, which influence the stress distribution and consequently the taut regions. Thus, the model successfully captures how the material stiffens in response to magnetic stimuli, enhancing the load-carrying capacity of the membrane. It can be concluded that while the model does not explicitly define stiffness as a function of electric or magnetic field, it inherently reflects field-modulated stiffness effects through the deformation behavior and evolution of taut domains. The shrinking or expansion of these regions under different electromagnetic loading conditions serves as a clear indicator of effective stiffness variations, governed by both material microstructure and external actuation fields.

The difference in deformation behavior under magnetic and electric loading arises from the distinct nature of the actuation mechanisms associated with magnetoactive and electroactive elastomers (Huang et al., 2024; Roghani et al., 2025). (1) In electroactive materials, forces act through the thickness leading to lateral contraction in taut zones. (2) In magnetoactive systems, forces can act along or perpendicular to the surface, often leading to local bulging or expansion in regions under tension. This contrast highlights the fundamentally different ways magnetic and electric fields interact with soft materials, and supports the complementary simultaneous exploitation of these stimuli in multifunctional soft actuators.

The aforementioned beneficial effect of applied magnetic and electric fields can be illustrated in the context of energy harvesting systems, as depicted in Fig. 7. In this system, fixed charges on the top and bottom layers of the elastomeric film are stored as an output through an applied input pressure. Under mechanical loading, the film undergoes thinning and area expansion, resulting in a large capacitance and low voltage generation in the absence of a magnetic field. However, when a magnetic field is applied, the film experiences an increase in thickness and a decrease in area. As a result, a higher voltage state is achieved, leading to a reduction in capacitance (Alameh et al., 2018; Kumar & Sarangi, 2018). By utilizing this configuration, it becomes possible to achieve a new elevated power state through the application of a magnetic field. Compared to the previous lower power level, the higher power state generated by the application of a magnetic field allows for increased power generation in the energy harvesting process for the same connected membrane.

Hence, it is observed that when the smart membrane is subjected to a constant magnetic field, the entanglement parameter significantly alters the critical lateral stretch and electric field of the membrane. The critical activation parameter e_{crit} corresponds to the maximum achievable stretch of the membrane, indicating that the membrane cannot undergo any further stretching beyond this threshold. In line with that, we plotted a graph (Fig. 8), depicting the effect of entanglement parameter on the critical lateral stretch and electric field of the membrane. The lateral stretches are obtained at the critical applied electric field where the taut

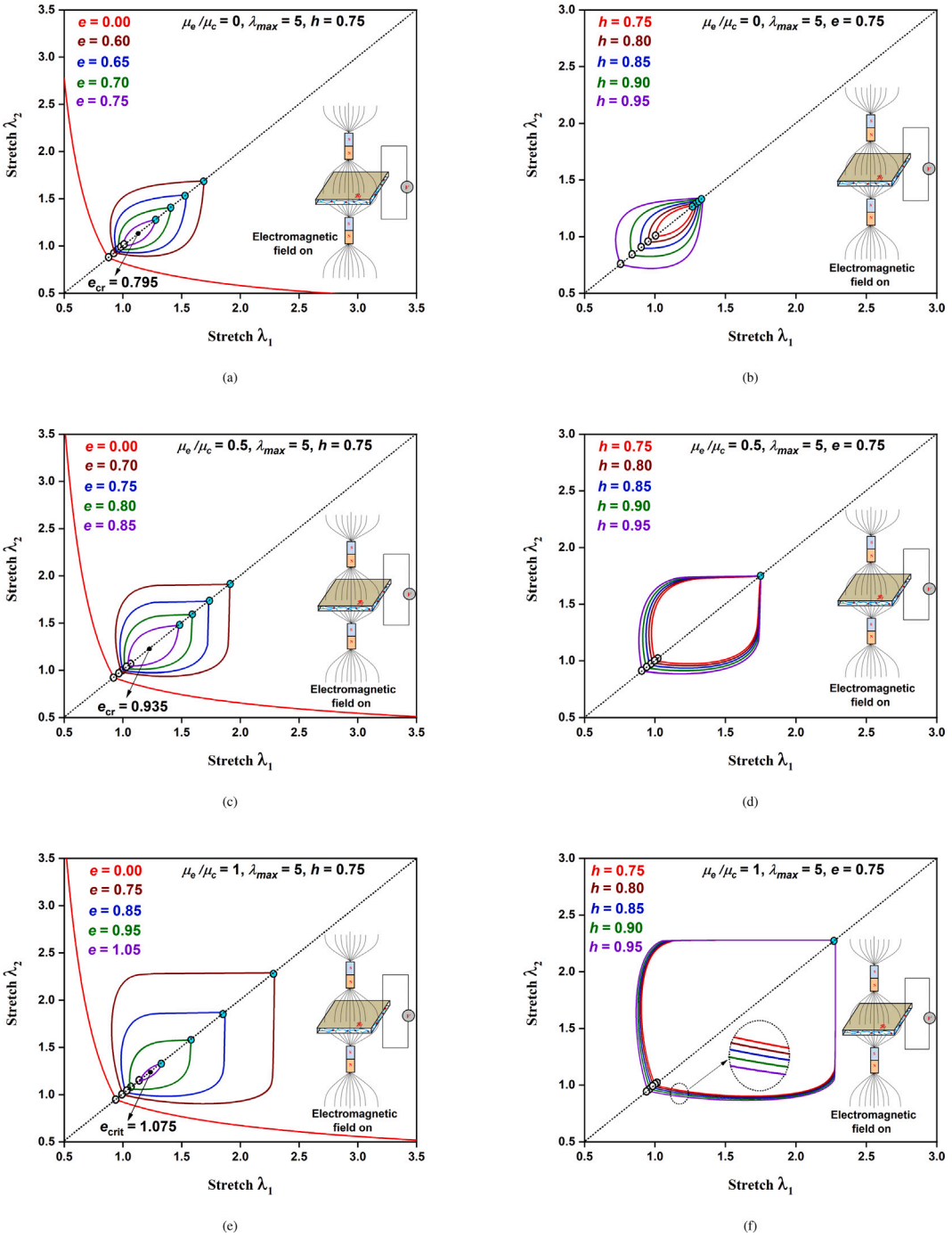

Fig. 6. Taut state curves of smart thin membrane for three different levels of entanglement parameter (μ_e/μ_c = 0.0, 0.5, and 1.0) subjected to (a, c, e) different levels of electric field e at constant magnetic field h= 0.75, and (b, d, f) different levels of magnetic field h at constant electric field e = 0.75, with λ_{max} = 5.

region shrinks to a point at a certain magnetic field level h. As anticipated, Fig. 8 indicates that the membrane having a larger entanglement parameter requires higher activation (e_{crit}) and also generates maximum lateral stretch (λ_{crit}) in the membrane.

We plot the stress–stretch characteristics (using Eq. (17)) of a smart elastomer in an equibiaxial state to examine the impact of polymer chains entanglements for applied electromagnetic field, as depicted in Fig. 9. To provide a comprehensive reference, the stress–strain characteristics for the previously discussed conditions (see Figs. 6(a, c, e)) are evaluated and shown in Figs. 9(a,

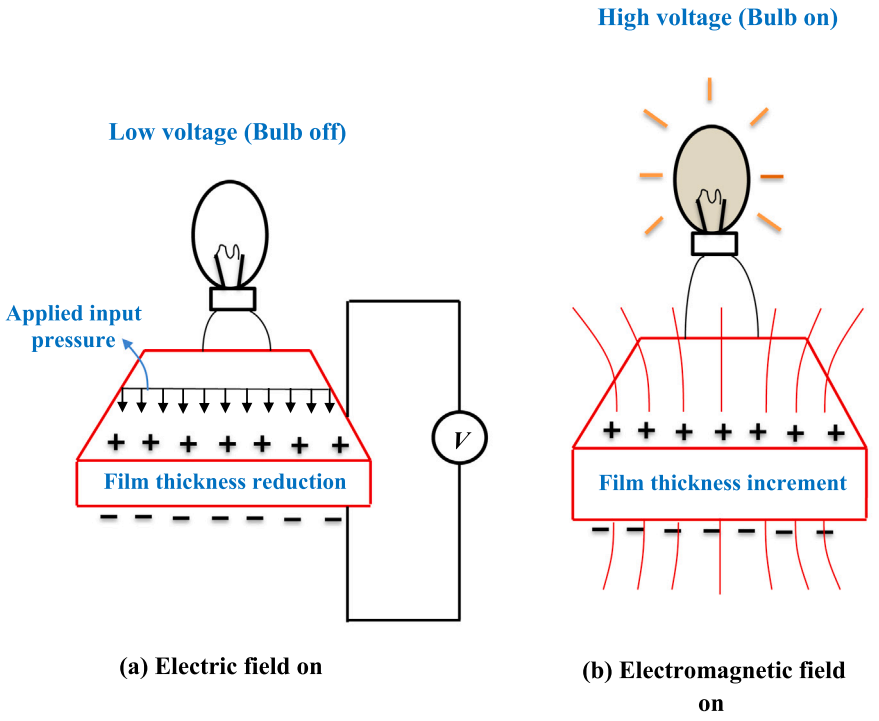

Fig. 7. A schematic representation of the smart membrane-based energy harvesting system triggered by (a) electrical actuation, and (b) electromagnetic actuation.

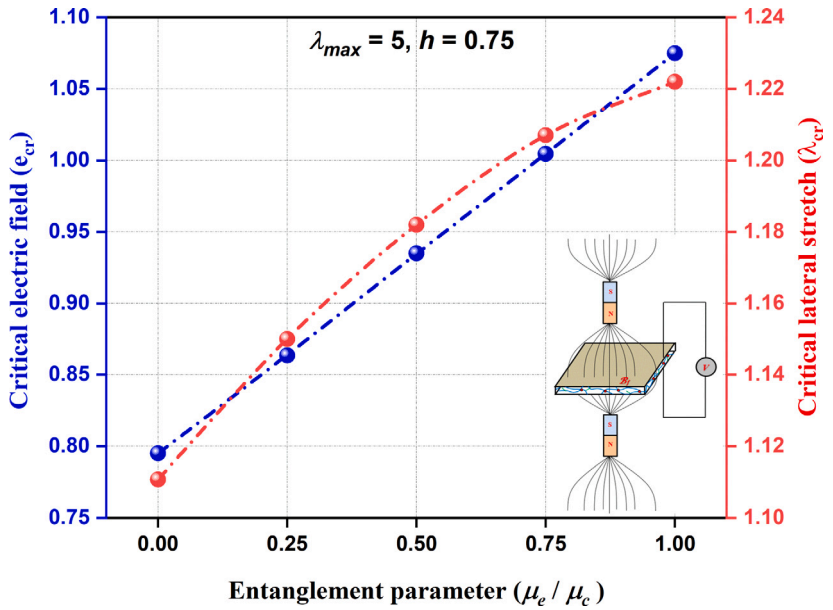

Fig. 8. Effect of entanglement parameter on the critical lateral stretch and critical electric field of a smart membrane under magnetic loading condition (h = 0.75) with λ_{max} = 5. The schematic included as inset here is intended to conceptually represent the application of combined electromagnetic fields to the membrane. Its purpose is illustrative, aiming to serve as a visual cue to reinforce the context of coupled field actuation.

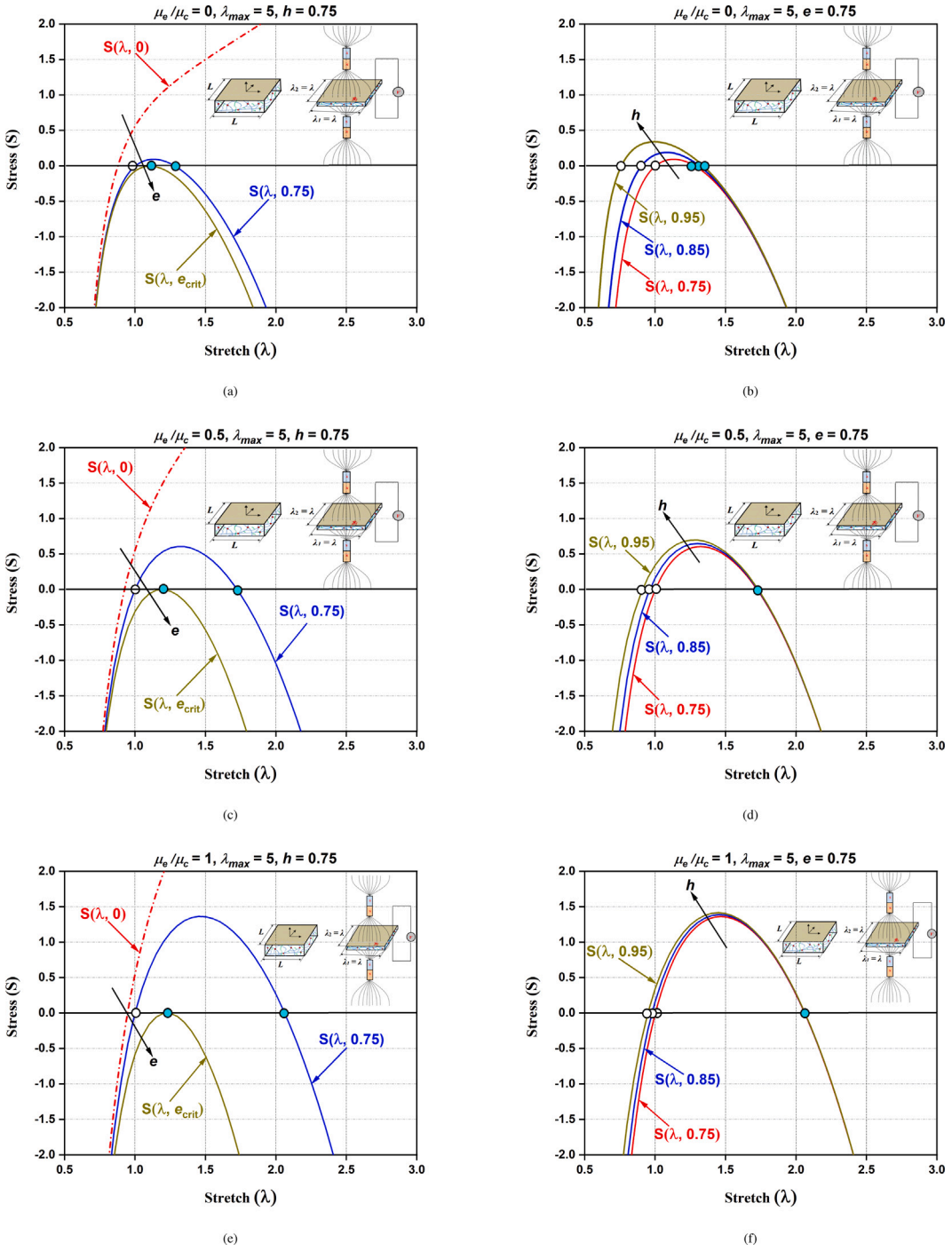

Fig. 9. Stress–stretch curves of smart thin membrane under equibiaxial condition for three different levels of entanglement parameter (μ_e/μ_c = 0.0, 0.5, and 1.0) subjected to (a, c, e) different levels of electric field e at constant magnetic field h= 0.75, and (b, d, f) different levels of magnetic field h at constant electric field e = 0.75, with λ_{max} = 5. The schematic included as inset here is intended to conceptually represent the application of combined electromagnetic fields to the membrane. Its purpose is illustrative, aiming to serve as a visual cue to reinforce the context of coupled field actuation and the resulting deformation behavior.

c, e). From these figures, it can be observed that for an applied magnetic field, both of the solutions of Eq. (17) merge into a single point (shown via. filled circle) when the activation field e reaches the critical threshold e_{crit} = 0.795, 0.935, and 1.075 for entanglement parameters μ_e/μ_c = 0.0, 0.5, and 1.0, respectively. Beyond this critical threshold, no additional equilibrium solutions

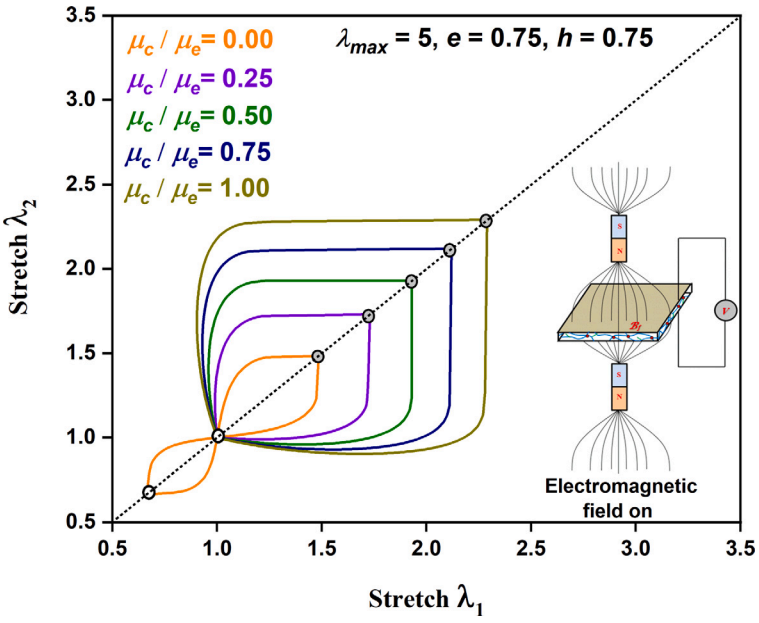

Fig. 10. Taut state curves of a smart elastomer for different crosslink parameter (μ_c/μ_e) subjected to an electromagnetic field ($e = 0.75$, $h = 0.75$) with $\lambda_{max} = 5$.

exist. This absence of equilibrium is commonly observed and well-documented in experimental literature, referred to as the Pull-in instability (Blok & LeGrand, 1969; Díaz-Calleja et al., 2008; Pelrine et al., 2000; Sharma et al., 2021; Zhao & Suo, 2009). Similarly, Figs. 9(b, d, f) depict the stress–strain characteristics for different levels of magnetic field under the conditions stated in Figs. 6(b, d, f). It is evident from these figures that there are two equilibrium states corresponding to all applied magnetic field values. The higher equilibrium states, shown by filled circles, remain consistent for entangled membranes ($\mu_e/\mu_c = 0.5$ and 1.0), indicating that they depend solely on the applied electric field e and are independent of the magnetic field h. On the other hand, the lower equilibrium state, symbolized by unfilled circles is significantly influenced by the applied magnetic field for all entanglement parameter levels ($\mu_e/\mu_c = 0.0$, 0.5, and 1.0). Moreover, as the magnetic field strength increases, the magnitude of the lower equilibrium solution decreases.

3.3. Effect of polymer chain crosslinks

This subsection investigates the influence of polymer chain crosslinks on the taut states of the smart elastomer in terms of principal stretches, while maintaining a constant density of entanglements ($\mu_e = 1$). We vary the dimensionless crosslink parameter μ_c/μ_e from 0 to 0.25, 0.5, 0.75, and 1.0 (Davidson & Goulbourne, 2013; Zhu & Luo, 2017, 2018; Zhu et al., 2018) at a specific level of chain extensibility, denoted as $\lambda_{max} = 5$. To facilitate the analysis, we normalize Eqs. (11)–(12) with respect to μ_e, and introduce dimensionless electric and magnetic fields defined as follows:

$$e = E_0\sqrt{\frac{\varepsilon_0}{\mu_e}}, \quad h = H_0\sqrt{\frac{\alpha_0}{\mu_e}}. \tag{18}$$

By inserting the above-normalized expressions of the magnetic and electric field variables into the governing Eqs. (11)–(12), the following set of normalized equations are obtained:

$$\frac{\mu_c}{\mu_e}\left(\lambda_1^2 - \lambda_1^{-2}\lambda_2^{-2}\right)\left\{\frac{1}{3} + \frac{2\lambda_{\max}^2}{\left(3\lambda_{\max}^2 - \lambda_1^2 - \lambda_2^2 - \lambda_1^{-2}\lambda_2^{-2}\right)}\right\} + \left(\lambda_1 - \lambda_1^{-1} - \lambda_1^{-1}\lambda_2^{-1} + \lambda_1\lambda_2\right) - e^2\lambda_1^2\lambda_2^2 + h^2\lambda_1^{-2}\lambda_2^{-2} = 0, \tag{19}$$

$$S_{11}(\lambda, e, h) = S_{22}(\lambda, e, h) = S(\lambda, e, h) = \frac{\mu_c}{\mu_e}(\lambda - \lambda^{-5})\left\{\frac{1}{3} + \frac{2\lambda_{\max}^2}{\left(3\lambda_{\max}^2 - \lambda_1^2 - \lambda_2^2 - \lambda_1^{-2}\lambda_2^{-2}\right)}\right\} + \left(1 - \lambda^{-2} - \lambda^{-3} + \lambda\right) - e^2\lambda^3 + h^2\lambda^{-5}. \tag{20}$$

Here the focus is on investigating the impact of polymer chain crosslinks on the stretched states of a smart elastomer subjected to electromagnetic field. Initially, the impact of polymer chain crosslinks is studied for five aforementioned different sets of crosslink parameters denoted as μ_c/μ_e, as shown in Fig. 10. Additionally, the values of other variables are specified as $e = 0.75$, $h = 0.75$ and

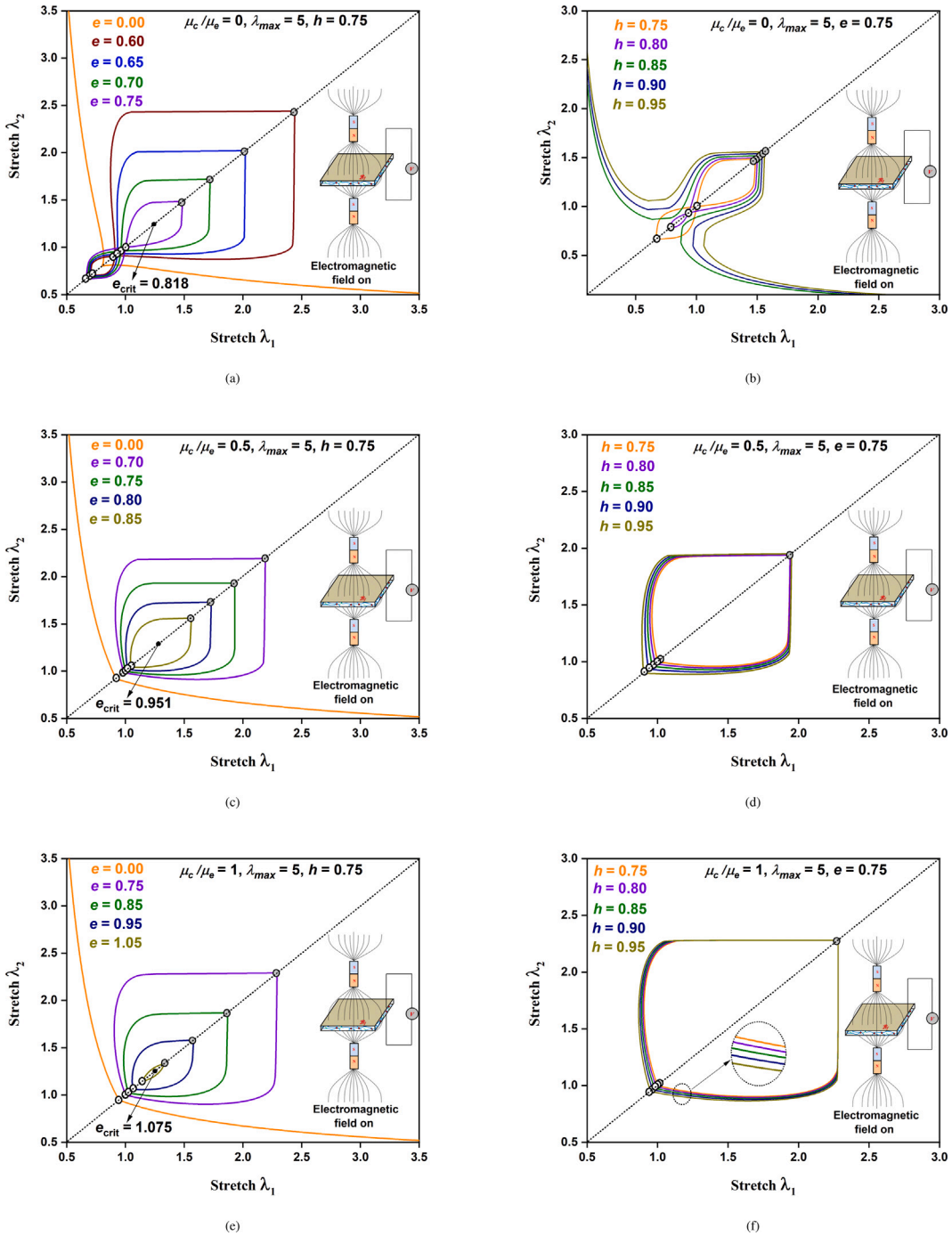

Fig. 11. Taut state curves of smart thin membrane for three different levels of crosslink parameter (μ_c/μ_e = 0.0, 0.5, and 1.0) subjected to (a, c, e) different levels of electric field e at constant magnetic field h= 0.75, and (b, d, f) different levels of magnetic field h at constant electric field e = 0.75, with λ_{max} = 5.

λ_{max} = 5. From the results depicted in Fig. 10, it is evident that the taut regions of the elastomer for an applied electromagnetic field enhance as the crosslink parameter is increased. This indicates that a higher crosslink parameter provides resistance to wrinkling or even suppresses the formation of wrinkles observed outside the taut domains (as illustrated in Fig. 2). Therefore, the introduction of enhanced polymer chain crosslinks demonstrates a prospective positive impact and holds promise as a design technique for surfaces that are wrinkle-resistant or wrinkle-free.

Figs. 11(a, c, e) illustrate the taut domain of a smart elastomer under varying crosslink parameters (μ_c/μ_e = 0.0, 0.5, and 1.0) and different levels of applied electric field, while maintaining a constant magnetic field (h = 0.75). Across all cases, as the applied electric field (e) increases, the taut region gradually diminishes until it reaches a critical activation point (e_{crit}). An intriguing observation is that when the crosslink parameter is zero (Fig. 11a), three equilibrium solutions exist. Generally, for the considered smart membrane, the taut region reduces to a single point at e_{crit} = 0.818, 0.951, and 1.075, corresponding to the crosslink parameters μ_c/μ_e of 0.0, 0.5, and 1.0, respectively. This behavior suggests that as the voltage rises, higher levels of crosslinking in the smart polymers require a greater electric field to undergo breakdown. It is worth highlighting that at higher voltage levels, no taut states are observed in any of the cases. Similarly, Figs. 11(b, d, f) present the taut behavior of a smart elastomer for the same three crosslink parameter levels mentioned earlier, but under varying levels of magnetic field while maintaining a constant applied electric field (e = 0.75). Unlike in the preceding example, the taut domains of the thin membranes expand as the applied magnetic loading increases, regardless of the level of polymer chain crosslinks. This indicates a beneficial effect of the applied magnetic field on the taut behavior. In particular, when the crosslink parameter is zero (Fig. 11d), only a single equilibrium state is observed. This means that at higher levels of applied magnetic field, there exists an upper equilibrium stretch, while no lower stretch state is observed.

We plot the stress–stretch characteristics (using Eq. (20)) of a smart elastomer in an equibiaxial state to examine the impact of polymer chains crosslinks for applied electromagnetic field, as depicted in Fig. 12. To provide a comprehensive reference, the stress–stretch responses for the previously discussed conditions (illustrated in Figs. 11(a, c, e)) are obtained and depicted in Figs. 12(a, c, e). From these figures, a noteworthy observation is that, for an applied magnetic field, both the solutions of Eq. (20) merge into a single point, shown by a filled circle. This occurs when the activation field e reaches the critical threshold of e_{crit} = 0.818, 0.951, and 1.075 for the respective crosslink parameters μ_c/μ_e of 0.0, 0.5, and 1.0. Specifically, at zero crosslink parameter (Fig. 12a), there exists three equilibrium solutions of the system when it is excited below the applied critical electric field. However, as the crosslink parameter increases, the system shows only two equilibrium states, indicating that the level of crosslink significantly alters the existence of the possible equilibrium state of the smart thin membrane.

Similarly, Figs. 12(b, d, f) depict the stress–stretch characteristics for different levels of magnetic field under the conditions stated in Figs. 11(b, d, f). It is evident that for zero crosslink parameter (Fig. 12b), there exists only one equilibrium state, i.e., upper equilibrium stretch state when the structure is excited by a higher level of magnetic field. However, it is observed that when a higher value of crosslink parameter is considered (Figs. 12(d, f)) there exist two equilibrium solutions for all applied magnetic field levels. The upper equilibrium solutions, represented by filled circles, remain consistent for crosslinked membranes (μ_c/μ_e = 0.5 and 1.0), indicating that they depend solely on the applied electric field e and are independent of the magnetic field h. On the other hand, the lower equilibrium solution, denoted by empty circles, is appreciably influenced by the applied magnetic field for all crosslink parameter levels (μ_c/μ_e = 0.0, 0.5, and 1.0). Moreover, as the magnetic field strength increases, the magnitude of the lower equilibrium solution decreases, indicating an appreciable effect of applied magnetic field on the lower equilibrium stretch state of the smart membrane.

3.4. Effect of polymer chain finite extensibility

As mentioned earlier, the polymer chains in smart elastomers have a limited length, which imposes a termination point on the extension of the elastomers. This finite extensibility of the polymer chains is a critical factor that influences the mechanical behavior of smart elastomers. Hence, this subsection investigates the effects of polymer chain finite extensibility on taut states of the smart membrane. We consider three varying degrees of polymer chain finite extensibility as λ_{max} = 2.5, 5 and 10. Subsequently, we have obtained the effect of λ_{max} for two different cases with entanglement parameter μ_e/μ_c = 0.5 (Fig. 13a), and crosslink parameter μ_c/μ_e = 0.5 (Fig. 13b) under the constant electromagnetic field ($e = h = 0.75$). In both the considered cases, the taut domain of the smart membrane shrinks as the finite extensibility λ_{max} of the smart membrane increases. This behavior can be attributed to the entropic elasticity formulation used in the constitutive model, which is grounded in the statistical mechanics of polymer networks. An increase in $\lambda_{\max}$ corresponds to polymer chains that can undergo greater stretch before reaching their configurational limit, resulting in a reduced entropic resistance to deformation. Consequently, the overall mechanical response leads to a contraction of the taut domain, as the membrane offers increased compliance in response to external stimuli. While the current model does not explicitly track a "curled" versus "uncurled" state, the effect emerges implicitly through the relationship between λ_{max} and the overall mechanical response of the membrane. The higher constraint at larger λ_{max} values is a result of increased configurational entropy, which limits further stretchability under external stimuli. The observed phenomenon suggests that when subjected to the same external stimulus, longer polymer chains tend to adopt a more curled or coiled conformation compared to shorter chains. This increased curling or coiling of longer chains results in a higher degree of constraining behavior at higher levels of chain finite extensibility.

We plot the stress–stretch characteristics of a smart thin membrane in an equibiaxial state to examine the impact of polymer chains finite extensibility for the two aforementioned cases (μ_e/μ_c = 0.5, μ_c/μ_e = 0.5), as depicted in Figs. 14(a–b). From these figures, it can be observed that for an applied constant electromagnetic loading, there exist two equilibrium solutions (shown by filled and empty circles) for all the considered levels of polymer chains finite extensibility. For both the considered cases, there exists a single lower equilibrium solution that satisfies the boundary condition mentioned in Eq. (14). However, the value of the upper equilibrium solution decreases with the increase in polymer chain finite extensibility. This suggests that the level of polymer chain finite deformation significantly alters the attained maximum equilibrium stretch of the smart membrane.

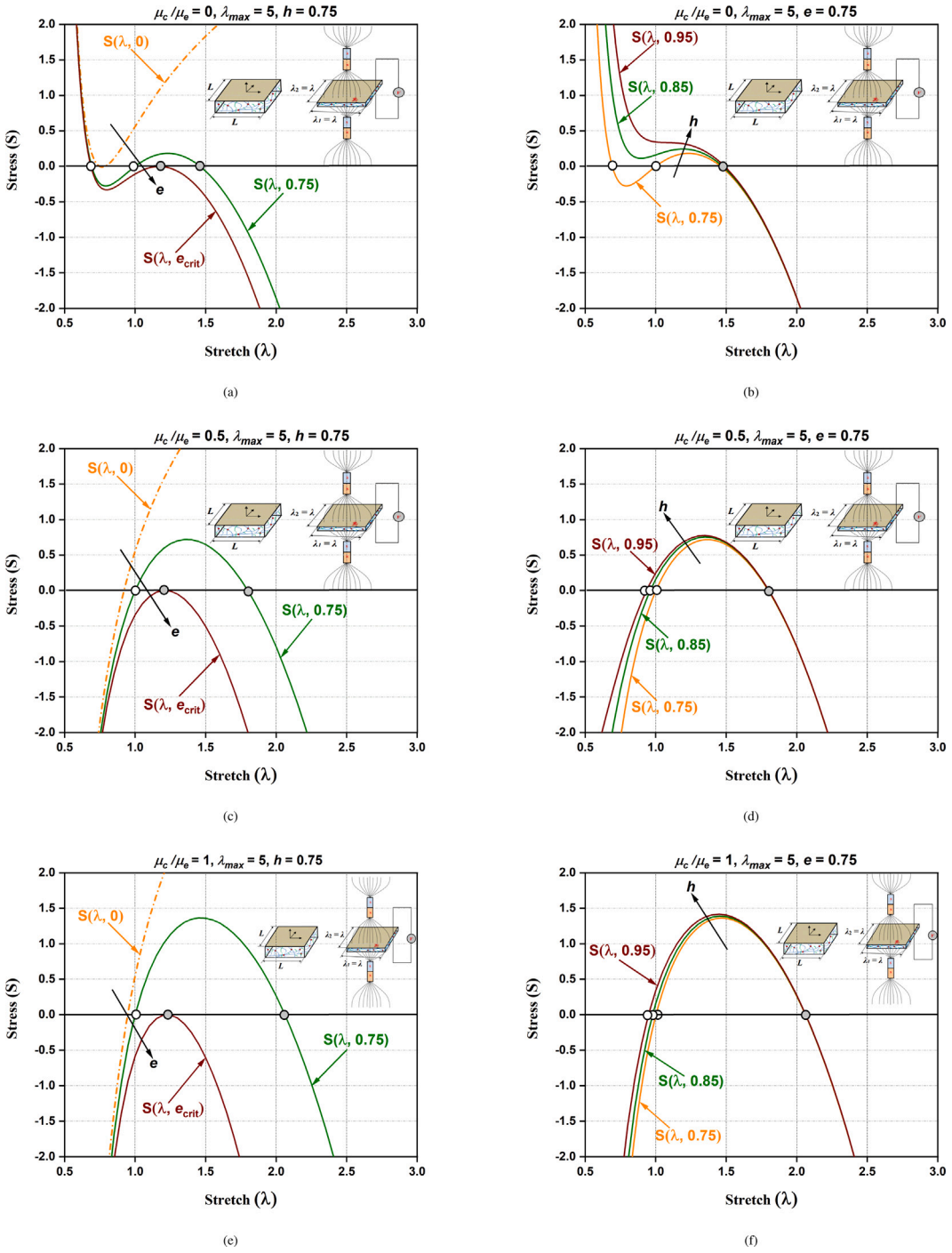

Fig. 12. Stress–stretch curves of smart thin membrane under equibiaxial condition for three different levels of crosslink parameter (μ_c/μ_e = 0.0, 0.5, and 1.0) subjected to (a, c, e) different levels of electric field e at constant magnetic field h= 0.75, and (b, d, f) different levels of magnetic field h at constant electric field e = 0.75, with λ_{max} = 5.

3.5. Critical remarks on the physical interpretation of model parameters, multiscale modeling and non-affine nature

Nature of the Model: The material model employed in our work is based on a physics-based non-affine network theory given by Davidson and Goulbourne (2013), rather than being purely phenomenological. It is best classified as a semi-phenomenological approach, as it incorporates fundamental micromechanical principles while also containing elements that require fitting to

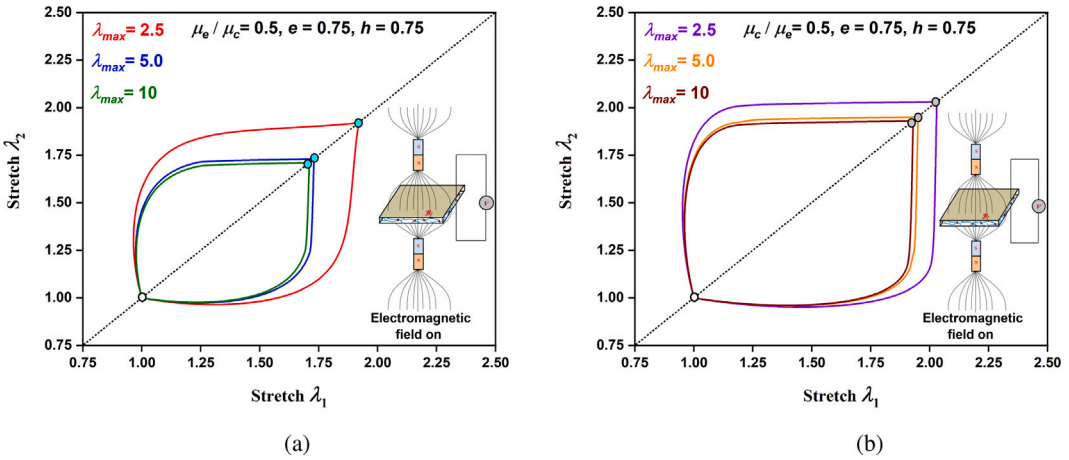

Fig. 13. Taut state curves of a smart membrane for varying degrees of polymer chain extensibility (λ_{max} = 2.5, 5 and 10) using constant (a) entanglement parameter μ_e/μ_c = 0.5, and (b) crosslink parameter μ_c/μ_e = 0.5, under applied electromagnetic field ($e = h$ = 0.75).

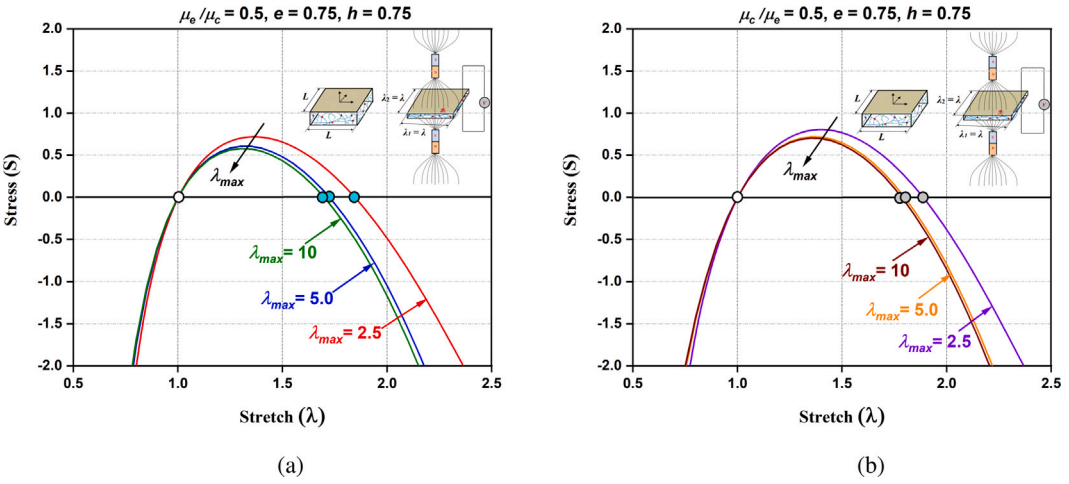

Fig. 14. Stress–stretch curves of a smart membrane for varying degrees of polymer chain extensibility (λ_{max} = 2.5, 5 and 10) using constant (a) entanglement parameter μ_e/μ_c = 0.5, and (b) crosslink parameter μ_c/μ_e = 0.5, under applied electromagnetic field ($e = h$ = 0.75).

experimental data. The model extends classical rubber elasticity theories by explicitly considering non-affine deformations and the contributions from both cross-linked and entangled network interactions.

The free energy density function adopted in our work is based on the model proposed by Davidson and Goulbourne (2013), which is a physics-based formulation that explicitly incorporates the effects of non-affine deformations at the microscale. Although the resulting strain energy density is expressed in terms of principal stretches, it reflects chain-level mechanics where the deformation of polymer segments deviates from purely affine assumptions. The incorporation of terms involving the chain extensibility parameter, the network modulus, and the entanglement modulus, encapsulates these non-affine characteristics. This justifies the use of the term non-affine in the current context, as the energy function captures the essential deviation from affine chain deformation that governs the mechanical response of such materials.

Physical Interpretation of Parameters: The coefficients in the free energy expression are linked to the polymer network structure as follows:

• Cross-link modulus (μ_c): This parameter is associated with the cross-link density (ρ_c) in the polymer network. Theoretically, it can be related to the classical rubber elasticity expression: $\mu_c = k_B \mathrm{T} \rho_c$, where k_B is the Boltzmann constant, T is the absolute temperature, and ρ_c represents the density of permanent cross-links in the network. This term dictates the resistance of the network to deformation.

• Entanglement modulus (μ_e): The parameter μ_e is connected to the entanglement density (ρ_e), which describes how frequently polymer chains physically interweave but are not chemically cross-linked. A similar relationship can be drawn: $\mu_e = k_B \mathrm{T} \rho_e$. However, in practical implementations, μ_e is often determined through fitting experimental stress–strain data, as entanglement effects are more complex and depend on molecular weight distribution, chain stiffness, and processing history.

• Maximum stretch limit (λ_{max}): This term accounts for the finite extensibility of polymer chains. It represents the natural stretch limit imposed by chain connectivity and excluded volume effects. In principle, λ_{max} can be inferred from molecular weight and Kuhn segment length, but in most cases, it is also treated as a fitted parameter.

Interdependence of Parameters: It is important to recognize that μ_c, μ_e, and λ_{max} are not entirely independent. Changes in network structure affect these parameters collectively:

• Increasing cross-link density (ρ_c) enhances μ_c, but it also affects entanglements by reducing chain mobility, potentially influencing μ_e.

• Entanglement effects (ρ_e) dominate in weakly cross-linked or physically cross-linked materials, contributing significantly to μ_e. However, in highly cross-linked systems, their role diminishes.

• λ_{max} is inherently linked to molecular weight between cross-links. Shorter network strands lead to lower λ_{max}, meaning that cross-linking and finite extensibility constraints are coupled.

Multiscale Modeling: The notion of multi-scale analysis here is intended to reflect the hierarchical physical considerations embedded in the model formulation, particularly the influence of microscopic phenomena, such as polymer chain crosslinking, entanglement density, and finite extensibility, on the macroscopic mechanical behavior. While the energy density is ultimately expressed in terms of macroscopic invariants, it is derived through a non-affine microstructurally motivated approach that captures essential chain-level mechanics, including deviations from affine deformation and field-coupled chain responses. In essence, the current modeling approach bridges micro-level interactions (cross-links, entanglements) with continuum-level mechanical response.

In summary, the current model is semi-phenomenological, integrating micromechanical principles with experimentally motivated parameterization. The parameters μ_c and μ_e are directly tied to network structure but often require fitting due to the complexities of real polymer networks. The parameters such as polymer crosslinking, entanglement, and finite extensibility play a crucial role in defining the mechanical response of electro-and magneto-active elastomers, and their regulation and determination in practical applications are indeed central to material design. In practical engineering applications, these parameters can be tuned through material formulation, processing techniques, and post-synthesis treatments to meet specific performance goals such as actuation range, response speed, or durability under cyclic loading. While exact quantification requires specialized experimental techniques, our model provides a useful framework for correlating these microscopic features with the macroscopic response, thereby guiding the rational design of next-generation smart materials.

3.6. Contributions, limitations and scope for future research

In this manuscript, we propose a continuum-based framework to investigate the influence of material-specific parameters (such as crosslinks, entanglements, and finite extensibility) and loading-specific parameters (such as electric and magnetic actuation) on the stability behavior of thin electro-magneto-active membranes. Our focus is on electro-magneto-mechanical instabilities such as Pull-in and wrinkling that signify the morphological instabilities in stretched membranes.

The broader motivation for this work stems from the potential utility of such instabilities in engineering applications, particularly scenarios involving controllable wrinkling, such as in acoustic metamaterials or optically tunable surfaces. For instance, prior studies, including our earlier work (Khurana et al., 2022), have demonstrated that biaxially stretched membranes can be driven into and out of wrinkled states through external fields, enabling reversible wrinkling. While this specific behavior is not modeled here, it highlights the importance of understanding how material and actuation parameters influence wrinkling onset and evolution.

Our analysis aims to delineate the boundaries of the taut region in the stretch-stretch space, thereby providing insight into how both material and loading features affect the stability response. Existing studies have often overlooked the combined influence of material-specific properties and coupled electro-magneto-mechanical loading. The novelty of our work lies in addressing these aspects by augmenting the strain–energy density function with additional physically motivated terms and systematically examining their individual effects.

We believe this unified approach offers valuable insights for the design of smart membrane systems where controlled instabilities may be functionally advantageous. While our approach draws inspiration from established literature, this study extends the existing computational frameworks in multiple significant and unprecedented exploitable directions, as discussed below:

Multiscale Perspective: Unlike prior studies, our work integrates a comprehensive multiscale analysis that explicitly incorporates cross-linking, entanglement, and finite extensibility, aspects that have not been systematically explored in this context. This provides a more refined understanding of the taut state mechanisms in active elastomers.

Experimental-Analytical Synergy: Our study not only validates the theoretical framework through well-controlled experiments but also provides new insights into the role of material microstructure in dictating macroscopic instabilities. This bridging of scales enhances the predictive capability of the model, which has practical implications for the design of soft active materials.

Integration of Magnetism and Electric Field Effects: The current model builds upon the elasticity formulation presented in literature (Davidson & Goulbourne, 2013), but extends it by explicitly incorporating magnetic field interactions. This inclusion is crucial for materials where magneto-electro-mechanical coupling plays a dominant role, such as in soft magnetoactive polymers or electro-magneto-responsive membranes. The presence of both electric and magnetic fields introduces additional stress contributions, which are carefully accounted for within the free energy formulation. This allows for a more precise prediction of field-induced deformations, a significant advancement over previous elasticity-based models.

Utilization of Taut Domains for Improved Predictability: A key aspect of our approach is the use of taut domain structures to describe the behavior of the membrane under combined mechanical, electrical, and magnetic loading. Taut domains refer to regions where the material experiences near-maximal local stretch, significantly affecting the overall mechanical stability and response

of the membrane. The incorporation of taut domain mechanics enables a more refined understanding of strain localization, stress distribution, and failure mechanisms. This is particularly important for thin films and soft materials, where localized deformations can drastically influence overall performance.

Enhanced Predictive Capability for Membrane Behavior: The study provides insights into how modulating the external fields (either electric or magnetic) can tailor mechanical properties, enabling tunable material responses — an aspect critical for applications in soft robotics, adaptive structures, and energy harvesting devices. The use of this physics-based approach ensures that the results are not purely empirical but rather grounded in fundamental material behavior, making the model generalizable to a broader class of electro-magneto-active materials. The present multi-field coupling enhances the model's applicability, providing a novel approach to understanding and controlling the mechanical response of smart materials under combined field influences.

Extended Applicability: The methodologies and findings of our work have broader applicability in emerging fields such as soft robotics, flexible electronics, and adaptive surfaces. While our focus is on electromagnetic elastomers, the principles we established here can be extrapolated to other material systems subjected to external stimuli.

Based on the above discussions, it becomes evident that the fundamental mechanics and theoretical advancements presented in this article have the potential to impact a broader range of engineering disciplines. However, a discussion on the limitations and applicability of the proposed model is important for providing a balanced perspective for guiding future use and development. Specifically, we acknowledge the following points: (1) The current model assumes idealized material homogeneity and isotropy at the macroscopic scale, whereas electro-/magneto-active elastomers may exhibit spatial variations in filler distribution or anisotropy due to fabrication methods. (2) Our current framework relies on quasi-static conditions and does not explicitly incorporate rate-dependent (viscoelastic) and time-dependent effects, which can be significant under dynamic loading or in high-frequency actuation. (3) The parameter values related to crosslinking, entanglement, and finite extensibility are representative and not derived from specific experimental datasets, making the model representative for qualitative predictions or design exploration unless calibrated with material-specific data. (4) The model currently considers planar membranes and does not yet extend to complex 3D geometries or non-uniform fields, which would be required for more advanced applications.

Despite these limitations, the model provides a robust and physically-informed framework to explore the multi-scale, non-affine mechanics of smart elastomers under coupled electro-magneto-mechanical loading. It offers valuable insights into the interplay between microscale features and macroscopic behavior, making it applicable for material design, prototyping, and early-stage actuator development. The above discussions will help clarify the scope and encourage further developments, building on this foundation.

4. Conclusions and perspective

This article introduces a continuum based multi-scale computational framework for effectively predicting the thresholds of taut domains in smart electro-magneto-active thin membranes incorporating the fundamental microcosmic features like crosslinks, entanglements, and finite extensibility of the polymer chains. By considering the concept of natural width under simple tension, a coupled nonlinear equation is derived to evaluate the taut domains.

In general, actuation devices fabricated using smart polymers often exhibit wrinkling and pull-in instability when they are subjected to external stimulation. These instabilities can disrupt the intended functionality of the actuation devices and hinder their reliability. The underlying reason for these instabilities is the complicated architecture of the polymer network, which results in a complex and chaotic arrangement of crosslinks and entanglements in smart elastomer membranes. This convoluted structure significantly influences the mechanical behavior of the polymers when external forces are applied. To better understand and characterize these instability phenomena, we have developed a physics-based non-affine material model incorporating the effects of critical factors like polymer chain crosslinks, entanglements, and finite extensibility.

Several noteworthy findings have been unveiled in this paper based on the numerical results. An increase in the entanglement and crosslink parameters leads to an expansion of the taut domains in smart actuator when subjected to an electromagnetic loading. Conversely, the taut domains decrease as the finite extensibility of the polymer chain increases under the same applied electromagnetic field. Smart membrane with higher entanglement and crosslink parameters requires a higher electric field for breakdown under a constant magnetic field. The study further reveals that for an applied constant magnetic loading, the taut domains diminish as the level of electrical loading applied to the membranes increases for all the considered levels of crosslink and entanglement density of the polymer chains. On the flip side, elevating the magnetic loading level effectively amplifies the taut domains within smart thin membranes when subjected to an applied electric field. This behavior holds true across all examined levels of entanglement and crosslink density, highlighting the beneficial impact of the applied magnetic field on the taut domain characteristics in smart thin membranes.

In summary, we establish that the size of taut domains in smart thin membranes can be tuned by adjusting the levels of polymer chain entanglements, crosslinks, and finite extensibility, as well as the applied electromagnetic loading conditions. In this context, we have developed an accurate, experimentally verified and insightful computational framework for numerical quantification and multi-scale bridging of structure–property relationships. Based on the proposed framework, it is possible to control the extent of the taut domains in smart membranes by engineering the microcosmic fundamental parameters in a multi-scale bottom-up framework. The insights gained from this research have the potential to revolutionize the design and optimization of electro-magneto-active thin membranes based on the exploitable convolution of intricate properties of polymer chains to meet specific application demands of advanced structural systems across the length scales.

CRediT authorship contribution statement

Aman Khurana: Writing – original draft, Investigation, Formal analysis, Data curation, Conceptualization. **Susmita Naskar:** Writing – review & editing, Project administration, Formal analysis. **M.M. Joglekar:** Resources, Investigation. **Tanmoy Mukhopadhyay:** Writing – review & editing, Supervision, Methodology, Conceptualization.

Declaration of competing interest

The authors declare that they have no known competing financial interests or personal relationships that could have appeared to influence the work reported in this paper.

Acknowledgments

The authors are very grateful to the editor and anonymous reviewers for their valuable comments. TM and SN would like to acknowledge the initiation grant received from the University of Southampton, United Kingdom during the period of this research. AK acknowledges the financial support provided by the Department of Science and Technology (DST), Government of India through Grant No. DST/INSPIRE/04/2022/001174.

Data availability

Data will be made available on request.

References

Agrawal, A., & Khurana, A. (2025). Unveiling the dynamics of particle-reinforced electro-magneto-active circular membrane. *International Journal of Non-Linear Mechanics*, Article 105064.

Agrawal, A., Khurana, A., & Kumar, D. (2025). Dynamics of an electric field vulnerable morpho-elastic biological membranes. *Journal of Applied Mechanics*, *92*, 1–041006.

Alameh, Z., Yang, S., Deng, Q., & Sharma, P. (2018). Emergent magnetoelectricity in soft materials, instability, and wireless energy harvesting. *Soft Matter*, *14*(28), 5856–5868.

Alblas, J. (1974). Electro-magneto-elasticity. In *Topics in applied continuum mechanics: symposium vienna, March 1–2, 1974* (pp. 71–114). Springer.

Bandopadhya, D., Bhattacharya, B., & Dutta, A. (2007). Modeling of hybrid damping scheme using smart magnetostrictive composites for flexible manipulator. *Journal of Reinforced Plastics and Composites*, *26*(9), 861–880.

Bardzokas, D. I., Filshtinsky, M. L., & Filshtinsky, L. A. (2007). *Mathematical methods in electro-magneto-elasticity*: *vol. 32*, Springer Science & Business Media.

Behera, S. K., Kumar, D., Maurya, C. S., & Sarangi, S. (2023). Universal rate-dependence in electro-magneto-active polymeric composites. *Composites Science and Technology*, *237*, Article 110015.

Blok, J., & LeGrand, D. (1969). Dielectric breakdown of polymer films. *Journal of Applied Physics*, *40*(1), 288–293.

Chen, V. W., Arora, N., Goshkoderia, A., Willey, C. L., Turgut, Z., Buskohl, P. R., Rudykh, S., & Juhl, A. T. (2023). Mechanical instability tuning of a magnetorheological elastomer composite laminate. *Composites Part B: Engineering*, *251*, Article 110472.

Christensen, L. R., Hassager, O., & Skov, A. L. (2019). Electro-thermal model of thermal breakdown in multilayered dielectric elastomers. *AIChE Journal*, *65*(2), 859–864.

Davidson, J. D., & Goulbourne, N. C. (2013). A nonaffine network model for elastomers undergoing finite deformations. *Journal of the Mechanics and Physics of Solids*, *61*(8), 1784–1797.

De Tommasi, D., Puglisi, G., Saccomandi, G., & Zurlo, G. (2010). Pull-in and wrinkling instabilities of electroactive dielectric actuators. *Journal of Physics D (Applied Physics)*, *43*(32), Article 325501.

De Tommasi, D., Puglisi, G., & Zurlo, G. (2011). Compression-induced failure of electroactive polymeric thin films. *Applied Physics Letters*, *98*(12), Article 123507.

De Tommasi, D., Puglisi, G., & Zurlo, G. (2012). Taut states of dielectric elastomer membranes. *International Journal of Non-Linear Mechanics*, *47*(2), 355–361.

Destrade, M., Saccomandi, G., & Sgura, I. (2017). Methodical fitting for mathematical models of rubber-like materials. *Proceedings of the Royal Society A: Mathematical, Physical and Engineering Sciences*, *473*(2198), Article 20160811.

Díaz-Calleja, R., Riande, E., & Sanchis, M. (2008). On electromechanical stability of dielectric elastomers. *Applied Physics Letters*, *93*(10), Article 101902.

Fan, R. L., Zhang, Y., Li, F., Zhang, Y. X., Sun, K., & Fan, Y. Z. (2001). Effect of high-temperature curing on the crosslink structures and dynamic mechanical properties of gum and N330-filled natural rubber vulcanizates. *Polymer Testing*, *20*(8), 925–936.

Ghuku, S., Naskar, S., & Mukhopadhyay, T. (2025). Stimuli–responsive programmable mechanics of bi-level architected nonlinear mechanical metamaterials. *Mechanics of Materials*, *206*, Article 105333.

Gour, S., Kumar, D., Khurana, A., & Joglekar, M. (2025). Thermo-electro-magnetostrictive unequal-biaxial taut states in thin elastomeric membranes. *Proceedings of the Royal Society A*, *481*(2311), Article 20240320.

He, T., Zhao, X., & Suo, Z. (2009). Dielectric elastomer membranes undergoing inhomogeneous deformation. *Journal of Applied Physics*, *106*(8), Article 083522.

Huang, W., Kang, G., & Ma, P. (2024). Uniaxial electro-mechanically coupled cyclic deformation of VHB 4905 dielectric elastomer: experiment and constitutive model. *Journal of Materials Engineering and Performance*, *33*(6), 2952–2967.

Kanan, A., Klausler, W., & Kaliske, M. (2024). *On the Thermo-Mechanics of Electro-Active and Magneto-Active Polymers–Constitutive and Computational Modeling Approaches*. Elsevier.

Khurana, A., Joglekar, M., & Zurlo, G. (2022). Electromechanical stability of wrinkled dielectric elastomers. *International Journal of Solids and Structures*, *246*, Article 111613.

Khurana, A., Kumar, A., Raut, S. K., Sharma, A. K., & Joglekar, M. M. (2021). Effect of viscoelasticity on the nonlinear dynamic behavior of dielectric elastomer minimum energy structures. *International Journal of Solids and Structures*, *208*, 141–153.

Khurana, A., Kumar, A., Sharma, A. K., & Joglekar, M. (2021a). Effect of polymer chains entanglements, crosslinks and finite extensibility on the nonlinear dynamic oscillations of dielectric viscoelastomer actuators. *Nonlinear Dynamics*, *104*(2), 1227–1251.

Khurana, A., Kumar, D., Sharma, A. K., & Joglekar, M. M. (2021b). Nonlinear oscillations of particle-reinforced electro-magneto-viscoelastomer actuators. *Journal of Applied Mechanics*, *88*(12).

Khurana, A., Kumar, D., Sharma, A. K., & Joglekar, M. (2021c). Static and dynamic instability modeling of electro-magneto-active polymers with various entanglements and crosslinks. *International Journal of Non-Linear Mechanics*, Article 103865.
Khurana, A., Kumar, D., Sharma, A. K., Zurlo, G., & Joglekar, M. (2022). Taut domains in transversely isotropic electro-magneto-active thin membranes. *International Journal of Non-Linear Mechanics*, *147*, Article 104228.
Khurana, A., Zurlo, G., & Joglekar, M. (2022). Taut domain analysis of transversely isotropic dielectric elastomer membranes. In *ECCOMAS congress*.
Kleo, M., Förster-Zügel, F., Schlaak, H. F., & Wallmersperger, T. (2020). Thermo-electro-mechanical behavior of dielectric elastomer actuators: experimental investigations, modeling and simulation. *Smart Materials and Structures*, *29*(8), Article 085001.
Kumar, A., Khurana, A., Patra, A. K., Agrawal, Y., & Joglekar, M. (2023). Electromechanical performance of dielectric elastomer composites: Modeling and experimental characterization. *Composite Structures*, *320*, Article 117130.
Kumar, D., & Sarangi, S. (2018). Instability analysis of an electro-magneto-elastic actuator: A continuum mechanics approach. *AIP Advances*, *8*(11), Article 115314.
Kumar, D., & Sarangi, S. (2019a). Electro-magnetostriction under large deformation: modeling with experimental validation. *Mechanics of Materials*, *128*, 1–10.
Kundu, D., Ghuku, S., Naskar, S., & Mukhopadhyay, T. (2023). Extreme specific stiffness through interactive cellular networks in bi-level micro-topology architected metamaterials. *Advanced Engineering Materials*, *25*(8), Article 2201407.
Kundu, D., Naskar, S., & Mukhopadhyay, T. (2024). Active mechanical cloaking for unsupervised damage resilience in programmable elastic metamaterials. *Philosophical Transactions A*, *382*(2278), Article 20230360.
Li, K., Wu, W., Jiang, Z., & Cai, S. (2018). Voltage-induced wrinkling in a constrained annular dielectric elastomer film. *Journal of Applied Mechanics*, *85*(1), Article 011007.
Li, B., Zhang, J., Chen, H., & Li, D. (2016). Voltage-induced pinnacle response in the dynamics of dielectric elastomers. *Physical Review E*, *93*(5), Article 052506.
Machado, M. R., Moura, B., Dey, S., & Mukhopadhyay, T. (2022). Bandgap manipulation of single and multi-frequency smart metastructures with random impedance disorder. *Smart Materials and Structures*, *31*(10), Article 105020.
Mehnert, M., Hossain, M., & Steinmann, P. (2021a). A complete thermo–electro–viscoelastic characterization of dielectric elastomers, part I: Experimental investigations. *Journal of the Mechanics and Physics of Solids*, *157*, Article 104603.
Mehnert, M., Hossain, M., & Steinmann, P. (2021b). A complete thermo-electro-viscoelastic characterization of dielectric elastomers, part II: Continuum modeling approach. *Journal of the Mechanics and Physics of Solids*, *157*, Article 104625.
Mondal, S., Mukhopadhyay, T., & Naskar, S. (2025). Active heterogeneous mode coupling in bi-level multi-physically architected metamaterials for temporal, on-demand and tunable programming. *Communications Engineering*, *4*(1), 1–15.
Moreno-Mateos, M. A., Lopez-Donaire, M. L., Hossain, M., & Garcia-Gonzalez, D. (2022). Effects of soft and hard magnetic particles on the mechanical performance of ultra-soft magnetorheological elastomers. *Smart Materials and Structures*, *31*(6), Article 065018.
Pandey, A. K., Khurana, A., & Sharma, A. K. (2023). Dynamic modeling and residual vibration suppression of electrostatically driven soft dielectric elastomer minimum energy structures. *European Journal of Mechanics. A. Solids*, *100*, Article 104971.
Pandey, A. K., Khurana, A., & Sharma, A. K. (2024). Thermo-electro-mechanical effects on nonlinear dynamics of smart dielectric elastomer minimum energy structures. *European Journal of Mechanics. A. Solids*, *105*, Article 105222.
Patra, A. K., Khurana, A., & Kumar, D. (2024). Modeling and analysis of a thermo-electro-magneto-viscoelastic actuator. *International Journal of Applied Mechanics*, *16*(02), Article 2450015.
Patra, A. K., Khurana, A., Kumar, D., & Saxena, P. (2024). Impact of compliant electrodes on the dynamics of electromagnetoactive membranes. *International Journal of Non-Linear Mechanics*, Article 104906.
Pelrine, R., Kornbluh, R., Pei, Q., & Joseph, J. (2000). High-speed electrically actuated elastomers with strain greater than 100%. *Science*, *287*(5454), 836–839.
Plante, J.-S., & Dubowsky, S. (2006). Large-scale failure modes of dielectric elastomer actuators. *International Journal of Solids and Structures*, *43*(25–26), 7727–7751.
Puglisi, G., & Saccomandi, G. (2015). The gent model for rubber-like materials: an appraisal for an ingenious and simple idea. *International Journal of Non-Linear Mechanics*, *68*, 17–24.
Puglisi, G., & Saccomandi, G. (2016). Multi-scale modelling of rubber-like materials and soft tissues: an appraisal. *Proceedings of the Royal Society A: Mathematical, Physical and Engineering Sciences*, *472*(2187), Article 20160060.
Qin, B., Zhong, Z., & Zhang, T.-Y. (2023). A thermo-electro-viscoelastic model for dielectric elastomers. *Materials*, *16*(17), 5917.
Rabczuk, T., Ren, H., & Zhuang, X. (2023). Nonlocal operator method for computational electromagnetic field and waveguide problem. In *Computational methods based on peridynamics and nonlocal operators: theory and applications* (pp. 99–122).
Roghani, M., Romeis, D., Glavan, G., Belyaeva, I. A., Shamonin, M., & Saphiannikova, M. (2025). Magnetically induced deformation of isotropic magnetoactive elastomers and its relation to the magnetorheological effect. *Physical Review Applied*, *23*(3), Article 034041.
Sharma, A. K., & Joglekar, M. (2018). Effect of anisotropy on the dynamic electromechanical instability of a dielectric elastomer actuator. *Smart Materials and Structures*, *28*(1), Article 015006.
Sharma, A. K., Khurana, A., & Joglekar, M. M. (2021). A finite element model for investigating the thermo-electro-mechanical response of inhomogeneously deforming dielectric elastomer actuators. *European Journal of Computational Mechanics*, *30*, 387–408.
Sharma, A., Naskar, S., & Mukhopadhyay, T. (2025). Multi-physically programmable tubular origami metamaterials: Exploitable nexus of geometry, folding mechanics and stimuli-responsive physics.
Sharma, B. L., & Saxena, P. (2021). Variational principles of nonlinear magnetoelastostatics and their correspondences. *Mathematics and Mechanics of Solids*, *26*(10), 1424–1454.
Shui, L., Liu, Y., Li, B., Zou, C., Tang, C., Zhu, L., & Chen, X. (2019). Mechanisms of electromechanical wrinkling for highly stretched substrate-free dielectric elastic membrane. *Journal of the Mechanics and Physics of Solids*, *122*, 520–537.
Singh, A., Mukhopadhyay, T., Adhikari, S., & Bhattacharya, B. (2022a). Active multi-physical modulation of Poisson's ratios in composite piezoelectric lattices: on-demand sign reversal. *Composite Structures*, *280*, Article 114857.
Singh, A., Mukhopadhyay, T., Adhikari, S., & Bhattacharya, B. (2022b). Extreme on-demand contactless modulation of elastic properties in magnetostrictive lattices. *Smart Materials and Structures*, *31*(12), Article 125005.
Sinha, P., & Mukhopadhyay, T. (2023). On-demand contactless programming of nonlinear elastic moduli in hard magnetic soft beam based broadband active lattice materials. *Smart Materials and Structures*, *32*(5), Article 055021.
Sinha, P., & Mukhopadhyay, T. (2023). Programmable multi-physical mechanics of mechanical metamaterials. *Materials Science and Engineering: R: Reports*, *155*, Article 100745.
Steigmann, D., & Pipkin, A. (1989). Finite deformations of wrinkled membranes. *The Quarterly Journal of Mechanics and Applied Mathematics*, *42*(3), 427–440.
Suo, Z., Zhao, X., & Greene, W. H. (2008). A nonlinear field theory of deformable dielectrics. *Journal of the Mechanics and Physics of Solids*, *56*(2), 467–486.
Thai, T. Q., Zhuang, X., & Rabczuk, T. (2023). Curved flexoelectric and piezoelectric micro-beams for nonlinear vibration analysis of energy harvesting. *International Journal of Solids and Structures*, *264*, Article 112096.
Wang, Z., Jiang, B., Zhang, Y., Li, X., Wang, Y., Shang, Y., & Zhang, H. (2022). Influence of crosslink density on thermal, mechanical and dielectric properties of cross-linked fluorinated poly (aryl ether) s. *European Polymer Journal*, *172*, Article 111244.
Wissler, M., & Mazza, E. (2005). Modeling and simulation of dielectric elastomer actuators. *Smart Materials and Structures*, *14*(6), 1396.
Wissler, M., & Mazza, E. (2007). Electromechanical coupling in dielectric elastomer actuators. *Sensors and Actuators A: Physical*, *138*(2), 384–393.

Yarali, E., Baniasadi, M., Bodaghi, M., & Baghani, M. (2020). 3D constitutive modeling of electro-magneto-visco-hyperelastic elastomers: a semi-analytical solution for cylinders under large torsion–extension deformation. *Smart Materials and Structures*, *29*(8), Article 085031.

Yarali, E., Baniasadi, M., Zolfagharian, A., Chavoshi, M., Arefi, F., Hossain, M., Bastola, A., Ansari, M., Foyouzat, A., Dabbagh, A., et al. (2022). Magneto-/electro-responsive polymers toward manufacturing, characterization, and biomedical/soft robotic applications. *Applied Materials Today*, *26*, Article 101306.

Zhang, J., Chen, H., & Li, D. (2018). Modeling nonlinear dynamic properties of dielectric elastomers with various crosslinks, entanglements, and finite deformations. *Journal of Applied Physics*, *123*(8), Article 084901.

Zhang, L., Wang, Y., Ren, J., Liu, X., Abdallaha, D., Wang, H., Song, X., Sun, H., Zhang, L., & Liu, J. Design magneto-dielectric elastomer composites for flexible electric/magnetic field response multi-mode sensors. *Polymer Composites*.

Zhao, X., & Suo, Z. (2009). Electromechanical instability in semicrystalline polymers. *Applied Physics Letters*, *95*(3), Article 031904.

Zhao, X., & Suo, Z. (2010). Theory of dielectric elastomers capable of giant deformation of actuation. *Physical Review Letters*, *104*(17), Article 178302.

Zhu, J., & Luo, J. (2017). Effect of entanglements on the electromechanical stability of dielectric elastomers. *Europhysics Letters*, *119*(2), 26003.

Zhu, J., & Luo, J. (2018). Effects of entanglements and finite extensibility of polymer chains on the mechanical behavior of hydrogels. *Acta Mechanica*, *229*, 1703–1719.

Zhu, J., Luo, J., & Xiao, Z. (2018). Snap-through instability analysis of dielectric elastomers with consideration of chain entanglements. *Materials Research Express*, *5*(6), Article 065307.

Zurlo, G., Destrade, M., DeTommasi, D., & Puglisi, G. (2017). Catastrophic thinning of dielectric elastomers. *Physical Review Letters*, *118*(7), Article 078001.